

1 **Spatiotemporal consistency of four gross primary production products and**
2 **solar-induced chlorophyll fluorescence in response to climate extremes**
3 **across CONUS in 2012**

4 **Xiaocui Wu¹, Xiangming Xiao^{1,2,*}, Yao Zhang¹, Wei He^{3,4}, Sebastian Wolf⁵, Jiquan**
5 **Chen⁶, Mingzhu He⁷, Christopher M. Gough⁸, Yuanwei Qin¹, Yanlian Zhou⁹, Russell**
6 **Doughty¹, Peter D. Blanken¹⁰**

7 1. Department of Microbiology and Plant Biology, Center for Spatial Analysis, University of
8 Oklahoma, Norman, OK 73019, USA

9 2. Ministry of Education Key Laboratory of Biodiversity Science and Ecological Engineering,
10 Institute of Biodiversity Science, Fudan University, Shanghai 200433, China.

11 3. International Institute for Earth System Science, Nanjing University, Nanjing, Jiangsu
12 210023, China

13 4. Center for Isotope Research (CIO), Energy and Sustainability Research Institute
14 Groningen (ESRIG), University of Groningen, Groningen, 9747 AG, The Netherlands

15 5. Department of Environmental Systems Science, ETH Zurich, 8092 Zurich, Switzerland

16 6. Center for Global Change & Earth Observations (CGCEO), Michigan State University,
17 East Lansing, MI 48823, USA

18 7. Numerical Terradynamic Simulation Group, College of Forestry & Conservation,
19 University of Montana, Missoula, MT 59812, USA

20 8. Virginia Commonwealth University, Department of Biology, 1000 W. Cary Street,
21 Richmond, VA 23284-2012, USA

22 9. Jiangsu Provincial Key Laboratory of Geographic Information Science and Technology,
23 School of Geographic and Oceanographic Sciences, Nanjing University, Nanjing, China

24 10. Department of Geography, University of Colorado Boulder, Boulder, Colorado, USA

25 Correspondence author: Xiangming Xiao (xiangming.xiao@ou.edu)

26 **Key Points:**

- 27 • The use of a C₃/C₄ fraction map derived from Cropland Data Layer (CDL) improves
28 gross primary production (GPP) estimates over croplands
- 29 • GPP estimates by Vegetation Photosynthesis Model are highly correlated with solar-
30 induced chlorophyll fluorescence (SIF)
- 31 • Increased GPP in the warm spring offset the reduced GPP by summer drought in
32 2012 over CONUS

33 **Abstract:** Large spatial-scale effects of climate extremes on gross primary production (GPP),
34 the largest terrestrial carbon flux, are highly uncertain even as these extremes increase in
35 frequency and extent. Here we report the impacts of spring warming and summer drought in
36 2012 on GPP across the contiguous US (CONUS) using estimates from four GPP models:
37 Vegetation Photosynthesis Model (VPM), MOD17A2H V006, Carnegie-Ames-Stanford
38 Approach (CASA), and Simple Biosphere/Carnegie-Ames-Stanford Approach (SiBCASA).
39 VPM simulations are driven by Moderate Resolution Imaging Spectroradiometer (MODIS),
40 North American Regional Reanalysis (NARR) climate data, and C₃ and C₄ cropland maps
41 from the United States Department of Agriculture (USDA) Cropland Data Layer (CDL)
42 dataset. Across 25 eddy covariance flux tower sites, GPP estimates from VPM (GPP_{VPM})
43 showed better accuracy in terms of cross-site variability and interannual variability ($R^2 = 0.84$
44 and 0.46, respectively) when compared to MOD17 GPP. We further assessed the spatial and
45 temporal (seasonal) consistency between GPP products and the Global Ozone Monitoring
46 Experiment-2 (GOME-2) solar-induced chlorophyll fluorescence (SIF) over CONUS during
47 2008-2014. The results suggested that GPP_{VPM} agrees best with SIF across space and time,
48 capturing seasonal dynamics and interannual variations. Anomaly analyses showed that
49 increased GPP during the spring compensated for the reduced GPP during the summer,
50 resulting in near-neutral changes in annual GPP for the CONUS. This study demonstrates the
51 importance of assessing the impacts of different types and timing of climate extremes on GPP,
52 and the need to improve light use efficiency models by incorporating C₃ and C₄ plant
53 functional types.

54 **Key words:** gross primary production; C₃ and C₄ cropland; solar-induced chlorophyll
55 fluorescence; Vegetation Photosynthesis Model; spring warming; drought

56 1. Introduction

57 Terrestrial ecosystems play a major role in the global carbon cycle, offsetting
58 approximately 25-30% of the CO₂ emitted by human activities since the 1950s (Le Quéré et
59 al. 2009). Gross primary production (GPP), the amount of CO₂ sequestered by vegetation
60 through photosynthetic assimilation before accounting for respiratory losses, is the largest
61 component of the global terrestrial carbon flux (Beer et al. 2010). Therefore, a small
62 fluctuation in GPP could have significant impact on atmospheric CO₂ concentrations.
63 However, the composition, structure, and functioning of terrestrial ecosystems are expected
64 to be substantially altered by increases in the duration or/and frequency of climate extremes
65 such as droughts, heatwaves, or intense precipitation events (Frank et al. 2015). It is a major
66 challenge to understand and project the response of terrestrial ecosystems to climate extremes
67 (Reichstein et al. 2013). In particular, droughts, together with the frequently co-occurring
68 heatwaves, are among the most widespread natural disasters, and could have large impacts on
69 annual GPP, ecosystem respiration, and net carbon balance (Frank et al. 2015; van der Molen
70 et al. 2011).

71 The impacts of climate extremes, especially heatwaves and droughts, on GPP have
72 been thoroughly investigated for selected events (Ciais et al. 2005; Parazoo et al. 2015; Wolf
73 et al. 2016; Yuan et al. 2016). However, how climate extremes affect the carbon cycle is still
74 poorly known at the landscape, regional, and global scales (Pan and Schimel 2016). To
75 investigate the impacts of climate extremes on GPP at ecosystem and landscape scales, three
76 approaches have been separately or jointly applied: eddy covariance (EC) flux tower
77 measurements (von Buttlar et al. 2017; Welp et al. 2007), remote-sensing data (Hilker et al.
78 2014), and biogeochemical models (Zscheischler et al. 2014). Since the 1990s, the EC flux
79 tower method has provided directly observed evidence for the seasonal changes of terrestrial

80 carbon fluxes, which increases our understanding of the underlying mechanisms of terrestrial
81 ecosystem responses and their feedbacks to climate extremes at the site scale (Reichstein et al.
82 2007). However, in-situ EC sites are limited by their relatively moderate-size footprints of
83 observation and the number and distribution of FLUXNET sites are limited, making it
84 difficult to assess the impacts of climate extremes on the carbon cycle at regional, continental,
85 and global scales. The GPP data derived from eddy covariance flux towers (GPP_{EC}), though
86 limited in their spatial coverage, are currently the best available data to validate GPP
87 estimates from process-based and data-driven GPP models. In contrast, optical and
88 microwave remote-sensing data provide larger scale insights into the vegetation structure,
89 including leaf area index, and light absorption by canopy (Chen 1996; Disney et al. 2006;
90 Ollinger 2011). Recently, solar-induced chlorophyll fluorescence (SIF) data have been
91 derived from satellite-based observations to estimate GPP, as it is tightly linked with
92 photosynthesis (Frankenberg et al. 2011; Porcar-Castell et al. 2014). However, SIF has a very
93 weak signal and accounts for about 2% of the total light absorbed by vegetation. Satellite
94 retrieved SIF measurements have comparatively large amounts of noise, and the recent SIF
95 data products are often aggregated in temporal and spatial domains resulting in a coarse
96 spatial and temporal resolution (monthly, $0.5^\circ \times 0.5^\circ$ for Global Ozone Monitoring Instrument
97 2, GOME-2) (Joiner et al. 2013). The coarse spatial resolution of SIF data products limits its
98 application because 0.5° gridcells (~ 50 km at Equator) are often highly heterogeneous. A
99 final approach uses terrestrial biosphere models to estimate GPP and ecosystem respiration
100 for a variety of ecosystems at multiple scales. However, the reliability of these models is
101 constrained by input datasets, model parameters, and model structures (Schaefer et al. 2012;
102 Schwalm et al. 2010). Hence, a synthesis and comparison of the different approaches can
103 reveal the shortcomings of individual approaches, and help to reach a more reliable

104 assessment of the multiple-scale responses of ecosystems to climate extremes ([Pan and](#)
105 [Schimel 2016](#)).

106 In 2012, the Contiguous United States (CONUS) experienced an abnormally warm
107 spring and dry summer ([Hoerling et al. 2014](#); [Knutson et al. 2013](#)). Record-breaking
108 temperatures were observed across 34 states during spring and a severe summer drought
109 followed, especially across the Great Plains and the Midwest Corn Belt. The 2012 US
110 drought was reported as one of the worst droughts since 1988 and had a comparable
111 magnitude and spatial extent of those during the 1930s and 1950s ([Hoerling et al. 2014](#);
112 [Rippey 2015](#)). Impacts of this spring warming and summer droughts on terrestrial carbon
113 fluxes in CONUS have been investigated, using the data from eddy covariance flux tower
114 sites, GPP from the MOD17 data product, and net ecosystem production (NEP) from
115 CarbonTracker (CTE2014 and CTE2015) ([Wolf et al. 2016](#)). They found that the losses of
116 NEP in the summer were offset by an unusually large increase of NEP in spring, resulting in
117 a small gain of annual NEP over CONUS (0.11 Pg C). They also reported that the decrease in
118 GPP during summer was much larger than the increase of spring GPP, resulting in a moderate
119 loss of annual GPP (-0.38 Pg C) over CONUS in 2012. However, there are large uncertainties
120 among the various GPP products ([Schaefer et al. 2012](#)); for example, the MOD17 GPP
121 product has large uncertainties in croplands ([Turner et al. 2006](#); [Xin et al. 2015](#)). Therefore,
122 there is a need to evaluate various GPP models and their GPP data products, which will help
123 us to better understand and assess GPP responses to spring warming and summer drought in
124 2012.

125 In this study, we analyzed GPP data products from four GPP models: (1) the
126 Vegetation Photosynthesis Model (VPM) ([Xiao et al. 2004a](#); [Xiao et al. 2004b](#)), which has
127 been well validated at both site ([Dong et al. 2015](#); [Doughty et al. 2018](#); [Jin et al. 2013](#); [Wagle](#)

128 [et al. 2015](#)) and regional scales ([Zhang et al. 2016a](#); [Zhang et al. 2017](#)) in previous studies. In
129 this study, we modified the model for cropland by separating C₃ and C₄ crops with detailed
130 Cropland Data Layer data; (2) MOD17 ([Running et al. 2004](#)), which is also used to evaluate
131 the 2012 spring warming and summer drought impact on GPP in [Wolf et al. \(2016\)](#); (3)
132 SiBCASA-GFED4 ([van der Velde et al. 2014](#)), and (4) CASA-GFED3 ([van der Werf et al.](#)
133 [2006](#); [van der Werf et al. 2010](#)). SiBCASA-GFED4 and CASA-GFED3 models are biosphere
134 models used in CarbonTracker Europe (CTE2014) ([van der Laan-Luijkx et al. 2017](#)) and
135 CarbonTracker (CT2014) ([Peters et al. 2007](#)), respectively, which provided the prior
136 biosphere carbon fluxes (NEP, GPP - Respiration) in the two carbon tracker systems. We
137 evaluated the GPP estimations from the four datasets with in-situ GPP data from eddy
138 covariance flux tower sites and SIF data from GOME-2. The objectives of this study are
139 threefold: (1) to demonstrate the potential of differentiating C₃ and C₄ croplands for
140 improving GPP estimates (using VPM as an example) and validate the GPP estimates against
141 FLUXNET data; (2) to quantify and understand the spatial-temporal consistency of GOME-2
142 SIF data and GPP estimates from various models; and (3) to assess the impacts of spring
143 warming and summer drought on GPP at the pixel, biome, and continental scales.

144 **2. Materials and Methods**

145 **2.1 Vegetation Photosynthesis Model (VPM)**

146 We used the VPM model ([Xiao et al. 2004a](#); [Xiao et al. 2004b](#)) to estimate GPP from
147 2008 to 2014 over CONUS. We followed the original model framework but further
148 differentiated between C₃ and C₄ croplands, since C₃ and C₄ crops have different maximum
149 light use efficiencies (ϵ_{\max}). The National Agricultural Statistics Service (NASS) Cropland
150 Data Layers (CDL) from the United States Department of Agriculture (USDA) were used to
151 calculate the area percentages of C₃ and C₄ croplands within each 500 m pixel over individual

152 years (Boryan et al. 2011). According to the USDA report, the major C₄ crop-types included
 153 corn, sorghum, sugarcane, and millet, and other crop-types were considered as C₃ croplands.
 154 The GPP of each pixel was estimated by area-weighted averaged GPP (Equation 1), which
 155 was derived from area fraction maps of C₃ and C₄ croplands and MCD12Q1 land use datasets:

$$156 \quad \text{GPP} = [(fC_3 \times \epsilon_{\max-C_3} + fC_4 \times \epsilon_{\max-C_4}) \times T_{\text{scalar}} \times W_{\text{scalar}}] \times \text{APAR}_{\text{chl}} \quad (1)$$

157 where fC_3 and fC_4 were the area fraction of C₃ and C₄ crops inside each cropland pixel,
 158 respectively. APAR_{chl} is photosynthetic active radiation (PAR) absorbed by chlorophyll in
 159 the canopy and is estimated from enhanced vegetation index (EVI) (Huete et al. 1997) as
 160 following:

$$161 \quad \text{APAR}_{\text{chl}} = 1.25 \times (\text{EVI} - 0.1) \quad (2)$$

162 This equation was modified from the previous model version (Xiao et al. 2004a; Xiao
 163 et al. 2004b), and has been applied in generating a global GPP product (Zhang et al. 2017).
 164 The coefficients 0.1 and 1.25 were used to adjust for sparsely vegetated or barren land and
 165 have been evaluated using the solar-induced chlorophyll fluorescence data.

166 The maximum light used efficiency values for C₃ croplands ($\epsilon_{\max-C_3}$) and C₄ croplands
 167 ($\epsilon_{\max-C_4}$) were specified as 0.035 mol CO₂ mol⁻¹ PAR (~1.8 g C m⁻² day⁻¹ MJ⁻¹ PAR), and
 168 0.053 mol CO₂ mol⁻¹ (PAR) (~ 2.7 g C m⁻² day⁻¹ MJ⁻¹ (PAR)) (1.5 times larger than C₃ types),
 169 respectively (Li et al. 2013). T_{scalar} and W_{scalar} are the temperature and water regulation factor
 170 and calculated as:

$$171 \quad T_{\text{scalar}} = \frac{(T-T_{\min})(T-T_{\max})}{[(T-T_{\min})(T-T_{\max})]-(T-T_{\text{opt}})^2} \quad (3)$$

$$172 \quad W_{\text{scalar}} = \frac{1+LSWI}{1+LSWI_{\max}} \quad (4)$$

173 where T is the air temperature, derived from the NCEP/NARR climate data. T_{min} , T_{max} , and
174 T_{opt} represent the minimum, maximum, and optimum temperatures for photosynthesis,
175 respectively, which are biome-specific and assigned values as in Zhang et al. (2016a).
176 $LSWI_{max}$ is the maximum land surface water index within the plant growing season, and we
177 applied a temporal smoothing method using nearby four years (two years before and two years
178 after) to eliminate potential bias (Zhang et al. 2017).

179 **2.2 Input datasets for VPM simulations in CONUS during 2008–2014**

180 Regional simulations of VPM model require climate, vegetation indices, and land
181 cover data. Here we briefly describe the input datasets used: (1) NCEP/NARR reanalysis
182 meteorological data, (2) MODIS surface reflectance and land cover data, and (3) NASS CDL
183 data.

184 **2.2.1 NCEP/NARR climate data**

185 The NCEP/NARR data was downloaded from (<http://www.esrl.noaa.gov/psd>). It
186 contains meteorological variables such as air temperature, precipitation, and downward
187 shortwave radiation from 1979 to present at a spatial resolution of 32 km and a temporal
188 resolution of 3 hours. The original 3-hourly NARR data were aggregated into daily data by
189 calculating the maximum, mean, and minimum air temperature in a day ($^{\circ}\text{C}$), and the
190 cumulative sum of downward shortwave radiation in a day. The resulting daily data were
191 further aggregated to 8-day intervals (following the MODIS 8-day temporal resolution) by
192 calculating the maximum, mean, and minimum temperature ($^{\circ}\text{C}$), and the cumulative sum of
193 downward shortwave radiation within an 8-day period. We also interpolated these climate
194 variables (32-km spatial resolution) to 500-m using the same algorithm reported in a previous
195 publication (Zhang et al. 2016a). As previous studies have shown, the NARR downward

196 shortwave radiation is systematically overestimated, so we adjusted it by applying a
197 correction factor of 0.8 as proposed in a previous study (Jin et al. 2015).

198 **2.2.2 MODIS surface reflectance and land cover product**

199 The latest version of MODIS surface reflectance product, MOD09A1 V006, was used
200 to calculate EVI (Huete et al. 1997) and Land Surface Water Index (LSWI) (Xiao et al.
201 2004b). A temporal algorithm was applied to EVI to gap-fill the missing data or bad-quality
202 data (Zhang et al. 2016a).

203 The MODIS land cover product (MCD12Q1 V005) provides annual global maps of
204 land cover at 500-m spatial resolution during 2001-2013 (Friedl et al. 2010). We used the
205 MCD12Q1 data at 2013 to represent year 2014. The IGBP land cover classification scheme
206 in the MCD12Q1 is used in this study (see Fig. 1a). The IGBP land cover map was then used
207 to derive biome-specific model parameter information for VPM simulations.

208 **2.2.3 USDA NASS CDL dataset**

209 Annual national CDL datasets with a spatial resolution of 30-m were available for our
210 study period (2008–2014)
211 (https://www.nass.usda.gov/Research_and_Science/Cropland/SARS1a.php). The CDL
212 datasets contain over 100 cropland types, and have very high classification accuracies for
213 most crops (over 90% accuracy for major crop types such as soybean and corn) (Boryan et al.
214 2011). For the VPM simulations, annual CDL datasets in 2008–2014 were aggregated to
215 generate data layers at 500-m spatial resolution that represent the ratio of C₃ and C₄
216 vegetation within individual 500-m gridcells for each year (Fig. 1b). The C₄ cropland layer
217 included corn, sorghum, sugarcane, and millet, and all other crops were C₃.

218 **2.3 Evaluation of GPP estimates during 2010–2014 from VPM**

219 **2.3.1 GPP data from eddy covariance flux tower sites**

220 Eddy covariance data from the FLUXNET2015 dataset were used to assess GPP_{VPM} .
221 We used 25 FLUXNET sites across CONUS according to their data availability during 2008–
222 2014, for which a summary about these sites is shown in Table 1 and Fig. 1a. The
223 FLUXNET2015 dataset used a standard workflow to process the data from the eddy
224 covariance flux tower sites (<http://fluxnet.fluxdata.org/data/>). The net ecosystem exchange
225 (NEE) of CO_2 between ecosystems and the atmosphere was gap-filled and then partitioned
226 into GPP and ecosystem respiration (ER) using two methods, the nighttime based and the
227 daytime based approaches (Lasslop et al. 2010; Reichstein et al. 2005). We calculated
228 average daily GPP_{EC} as the average of daily GPP estimated by the two methods. Then, we
229 calculated 8-day average GPP_{EC} by aggregating the average daily GPPs. For each 8-day
230 interval, only the shortwave radiation and net ecosystem exchange (NEE) observations with
231 more than 75% of good quality, gap-filled data were kept.

232

Figure 1 and Table 1 is here

233 We evaluated the seasonal and cross-site performance of GPP_{VPM} across biomes at 8-
234 day and interannual scales. We classified the land cover maps into four major types: forest
235 (FOR), grassland (GRA), cropland (CRO), and others (OTH) based on the MCD12Q1
236 landcover data. The evergreen needleleaf forest, evergreen broadleaf forest, deciduous
237 broadleaf forest, deciduous needleleaf forest, and mixed forest were lumped together as forest.
238 Grassland and cropland were the same classification scheme as MCD12Q1, while all the
239 other land cover types, such as savannas, shrublands, wetlands, and sparsely vegetated area,
240 were considered as OTH. To examine the ability of the model to capture the interannual
241 variability of GPP, we compared the anomaly of annual GPP for GPP_{EC} and GPP_{VPM} .
242 Specifically, we compared GPP_{VPM} and GPP_{MOD17} to the anomaly between GPP_{EC} in each
243 site year and average GPP_{EC} over all the site years for each site. The slope, root mean square
244 error (RMSE), and R^2 of the regression models were used to evaluate the difference between
245 modeled and eddy-covariance derived GPP.

246 **2.3.2 Solar-induced chlorophyll fluorescence (SIF) data from the GOME-2**

247 SIF is a very small amount of energy emitted by plants and has been demonstrated to
248 be highly correlated with GPP ([Guanter et al. 2014](#); [Wagle et al. 2016](#); [Zhang et al. 2016a](#)). In
249 this study, we used the monthly GOME-2 SIF data (V26) during 2008–2014 ([Joiner et al.](#)
250 [2013](#)). GOME-2 measurements are in the ultraviolet and visible part of the spectrum (240 -
251 790 nm) with a high spectral resolution between 0.2 and 0.5 nm and with the footprint size of
252 $80 \times 40 \text{ km}^2$. SIF is retrieved using a principle component analysis method in the 734 to 758
253 nm spectral window which overlaps the second peak of the SIF emission. The retrievals are
254 quality-filtered and aggregated into 0.5° grids and a monthly interval ([Joiner et al. 2013](#)).

255 2.4 Inter-comparison of GPP estimates among VPM and other three models

256 We compared GPP_{VPM} with the latest version of MOD17 GPP product (Running et al.
257 2004), MOD17A2H V006 (GPP_{MOD17}) at both site and regional scales. GPP_{MOD17} is estimated
258 at a spatial resolution of 500-m and a temporal resolution of 8-day, which matches the spatial
259 and temporal resolutions of GPP_{VPM} . MOD17 is also a LUE model and simulates GPP as the
260 product of $APAR_{canopy}$ and light use efficiency (ϵ_g). ϵ_g is determined by ϵ_{max} and scalars that
261 capture environmental limitations such as vapor pressure deficit and air temperature. ϵ_{max}
262 values are specific for different biome types (e.g., forest, shrub, grass, crop) (Running et al.
263 2004), but the product does not account for the differences of ϵ_{max} between C_3 and C_4
264 croplands, and ϵ_{max} for croplands is substantially too low (Turner et al. 2006; Xin et al. 2015).

265 We also compared GPP_{VPM} with GPP simulated by CASA-GFED3 (GPP_{CASA}). CASA
266 estimates Net Primary Productivity (NPP) based on the light use efficiency method (Monteith
267 1972, 1977) and further estimates GPP with an assumption $GPP = 2 * NPP$. ϵ_{max} for
268 predicting NPP in CASA is set uniformly ($0.55 \text{ g C MJ}^{-1} \text{ PAR}$) for different biomes (Potter et
269 al. 2012; Potter et al. 1993; Randerson et al. 1996). The CASA-GFED3 GPP product used a
270 calibrated ϵ_{max} for the Midwestern region, which was derived from crop yield observations,
271 meteorological data, and remotely sensed FPAR (Lobell et al. 2002), and thus corresponds
272 with much higher GPP values (roughly 45%) over the Midwestern US (Hilton et al. 2015).
273 GPP_{CASA} is used to generate prior biogenic CO_2 fluxes for the CarbonTracker system (Peters
274 et al. 2007) at a spatial resolution of $1^\circ \times 1.25^\circ$ every 3 hour. We resampled the data into $1^\circ \times 1^\circ$
275 and aggregated them into monthly values in this study.

276 The GPP estimates by the SiBCASA-GFED4 model ($GPP_{SiBCASA}$) (van der Velde et al.
277 2014) were also compared with regional GPP_{VPM} . $GPP_{SiBCASA}$ is used to generate prior
278 biogenic CO_2 fluxes in the Carbon Tracker Europe system (van der Laan-Luijkx et al. 2017).
279 SiBCASA combines the biophysical and GPP components from the Simple Biosphere model

280 (version 2.5) with the heterotrophic respiration (R_H) from CASA model, and calculates the
281 exchange of carbon, energy, and water at a temporal resolution of 10-min and at a spatial
282 resolution of $1^\circ \times 1^\circ$ (Schaefer et al. 2008; van der Velde et al. 2014). GPP is calculated for
283 both C_3 and C_4 plants by implementing a modified version of the C_3 enzyme kinetic model
284 (Farquhar et al. 1980) and the C_4 photosynthesis model (Collatz et al. 1992). The C_4
285 distribution map used in SiBCASA is a static map with the mean C_4 fraction in global $1^\circ \times 1^\circ$
286 grids (Still et al. 2003). The aggregated monthly $GPP_{SiBCASA}$ data is used for the comparison.

287 The impact of climate extremes on the GPP and SIF over the CONUS was evaluated
288 using the four GPP datasets and GOME-2 SIF data. The seasonal cycle and anomaly of
289 GPP_{VPM} , GPP_{MOD17} , $GPP_{SiBCASA}$, GPP_{CASA} and SIF in the year 2012 were compared to that in
290 the baseline year (the average of the year 2008, 2009, 2010, 2013 and 2014). The uncertainty
291 range of the anomaly was calculated as the standard deviation (SD) of the anomaly between
292 2012 and selected different baselines. We randomly chose at least three years from the year
293 2008, 2009, 2010, 2013 and 2014 to calculate the baseline, so there are 16 options ($C_5^3 + C_5^4$
294 $+ C_5^5$). As $GPP_{SiBCASA}$, GPP_{CASA} and SIF datasets have a spatial resolution of $1.0^\circ \times 1.0^\circ$, both
295 GPP_{VPM} and GPP_{MOD17} datasets (500-m spatial resolution) were aggregated to $1.0^\circ \times 1.0^\circ$. The
296 SIF data ($0.5^\circ \times 0.5^\circ$) was also aggregated to $1.0^\circ \times 1.0^\circ$. We then used the area-weighted
297 method to calculate annual total GPP ($Pg\ C\ year^{-1}$) and average SIF over CONUS.

298 3. Results

299 3.1 Seasonal dynamics and interannual variation of GPP at flux tower sites

300 GPP_{VPM} agreed reasonably well with the seasonal dynamics and peak values of
301 GPP_{EC} at most sites (Fig. 2). The coefficients of determination (R^2) varied from 0.32 (US-
302 SRC) site to 0.96 (US-Ne2 and US-UMB). GPP_{VPM} showed very high accuracy for the
303 cropland sites relative to GPP_{MOD17} (see Fig. 2 and Table 1). At the US-Ne1 and US-Ne2

304 maize sites, the regression between GPP_{VPM} and GPP_{EC} show a high R^2 value (> 0.95) and a
305 low RMSE value ($< 2.0 \text{ g C m}^{-2} \text{ day}^{-1}$), while the regression between GPP_{MOD17} and GPP_{EC}
306 show a moderate R^2 value (~ 0.50) and a large RMSE value ($7.0 \text{ g C m}^{-2} \text{ day}^{-1}$) (Table1).

307 At the 8-day scale, GPP_{VPM} agrees better with GPP_{EC} than does GPP_{MOD17} , and
308 GPP_{VPM} effectively captures the seasonal dynamics of GPP for all the four biomes (Fig. 3–a,
309 b). For croplands, GPP_{MOD17} shows significant underestimation with a slope of 0.37 while
310 GPP_{VPM} presents only slight underestimation with a slope of 0.97. The improvement in
311 GPP_{VPM} is most prominent in these C_4 cropland sites, such as US-Ne1 and US-Ne2 (Fig. 2
312 and Table 1), with peak value of GPP_{VPM} and GPP_{EC} in the growing season that are larger
313 than $20 \text{ g C m}^{-2} \text{ day}^{-1}$, while that of GPP_{MOD17} is less than $10 \text{ g C m}^{-2} \text{ day}^{-1}$. Across all 25 sites,
314 GPP_{VPM} explains about 84% of the seasonal dynamics of GPP_{EC} with RMSE of 1.7 g C m^2
315 day^{-1} , while GPP_{MOD17} only explains only about 55% with a RMSE value of $2.6 \text{ g C m}^{-2} \text{ day}^{-1}$.

316 **Figure 2 is here**

317 The interannual variation of GPP_{VPM} was best for croplands, followed by forest,
318 grasslands, and other biomes (Fig. 3c). In addition, the anomaly of annual GPP_{VPM} in
319 croplands, grasslands, and forest biomes has much higher consistency with GPP_{EC} than does
320 GPP_{MOD17} (Fig. 3–c, d). In other biomes (5 sites), both GPP_{VPM} and GPP_{MOD17} had relatively
321 low accuracy.

322 **Figure 3 is here**

323

324 **3.2 Spatial-temporal consistency between model-based GPP and SIF over CONUS in**
325 **the baseline years and drought year 2012**

326 We compared the spatial distribution of maximum monthly mean GPP ($\text{g C m}^2 \text{ day}^{-1}$)
327 from the four GPP products and annual maximum monthly mean SIF in the baseline year and
328 drought year 2012 at $1^\circ \times 1^\circ$ resolution (Fig.4 a–j). The maximum monthly mean GPP in 2008,
329 2009, 2010, 2013, and 2014 were used as baseline year. The three GPP products (GPP_{VPM} ,
330 GPP_{CASA} and $\text{GPP}_{\text{SiBCASA}}$) and SIF show the peak photosynthesis in the Mid-western corn-
331 belt region (Fig. 4a–j), which was consistent with the results reported by [Hilton et al. \(2017\)](#).
332 $\text{GPP}_{\text{MOD17}}$ did not have such a spatial pattern for maximum monthly GPP because it did not
333 include higher photosynthetic capacity for C_4 vegetation as did the other three models (VPM,
334 CASA and SiBCASA). Compared to the baseline years, most of gridcells had lower GPP and
335 SIF values during the drought in 2012. The correlation analysis (Fig. 5a–d; Fig. 5e–h)
336 showed that the maximum monthly GPP_{VPM} and SIF have the strongest linear relationship,
337 followed by $\text{SIF}/\text{GPP}_{\text{SiBCASA}}$, $\text{SIF}/\text{GPP}_{\text{CASA}}$, and $\text{SIF}/\text{GPP}_{\text{MOD17}}$.

338 
339

340 For annual total GPP, all four GPP products showed very similar spatial patterns with
341 SIF, with relatively high annual GPP ($> 1500 \text{ g C m}^{-2} \text{ year}^{-1}$) in the forested Southeastern US
342 and low annual GPP in the western regions where grasslands and deserts are dominant
343 (Fig. 4k–t). In 2012, GPP_{VPM} had a decrease in the Midwestern corn-belt region and Great
344 Plains, and an increase in the eastern temperate forest region, which is consistent with the
345 spatial patterns of SIF. Annual $\text{GPP}_{\text{MOD17}}$ had an obvious decrease in the Midwestern corn-
346 belt area but a slight increase in the eastern forest area in 2012. Annual $\text{GPP}_{\text{SiBCASA}}$ had no
347 significant differences between the baseline and drought year 2012. Annual GPP_{CASA} had

348 large increases in both the Midwestern corn-belt region and temperate forest area. The
349 correlation analysis (Fig. 5i-l) showed that annual GPP_{VPM} had a stronger linear relationship
350 with SIF ($R^2 = 0.94$) in the baseline years than $SIF/GPP_{SiBCASA}$ ($R^2 = 0.76$), SIF/GPP_{CASA} (R^2
351 $= 0.75$), and SIF/GPP_{MOD17} ($R^2 = 0.70$). We found similar results for the drought year 2012
352 (Fig. 5m-p), which suggested that the models performed similarly during baseline and
353 drought years.

354 **Figure 5 is here**

355
356 GPP estimates from all models had a high correlation with SIF (>0.9) in the wetter
357 eastern region but a low correlation in the dry western region, partly due to the very low SIF
358 signal and relatively large signal-to-noise ratio (Fig. 6 a-h). The percentages of the total
359 number of gridcells with a Pearson correlation coefficient larger than 0.9 in the baseline year
360 was $\sim 65\%$ for SIF/GPP_{VPM} , $\sim 55\%$ for SIF/GPP_{CASA} , $\sim 50\%$ for SIF/GPP_{MOD17} , and $\sim 47\%$ for
361 $SIF/GPP_{SiBCASA}$ (Fig. 6i-l). The four GPP models had no obvious differences in simulating
362 the seasonal dynamics of GPP between the baseline year and drought year 2012 (Fig. 6).

363 **Figure 6 is here**

364
365 The histograms of the slope values ($GPP = a \times SIF + b$) among these four GPP
366 models differed substantially. The slope values for the SIF/GPP_{VPM} were concentrated
367 between 4 and 7 $g\ C\ mW^{-1}\ nm^{-1}\ sr^{-1}$ ($\sim 53\%$ of all gridcells), while that for SIF/GPP_{MOD17}
368 were between 2 to 5 $g\ C\ mW^{-1}\ nm^{-1}\ sr^{-1}$ ($\sim 60\%$ of all gridcells). The slope values for the
369 SIF/GPP_{CASA} and $SIF/GPP_{SiBCASA}$ were more evenly distributed than that of SIF/GPP_{VPM} .
370 [Sun et al. \(2017\)](#) found the GPP-SIF relationship is consistent across different vegetation

371 types when comparing SIF with GPP_{EC} , but it is more divergent when comparing SIF with
372 modelled GPP because of the systematic GPP biases. The GPP-SIF slope for the four GPP
373 products in this study is also divergent over CONUS, but the VPM GPP-SIF slope is more
374 convergent than the other three models (Fig. 7).

375
376 **Figure 7 is here**

377 **3.3 Spatial-temporal consistency of GPP and SIF anomalies over CONUS in 2012**

378 To evaluate the impacts of spring warming and summer drought on GPP in 2012, we
379 compared the anomalies of GPP from GPP_{VPM} , GPP_{MOD17} , $GPP_{SiBCASA}$, and GPP_{CASA} to the
380 anomalies of SIF in the spring, summer, and the entire year at $1^\circ \times 1^\circ$ (latitude and longitude)
381 resolution (Fig. 8). The anomalies of GPP and SIF were calculated as the differences between
382 year 2012 and the baseline year. The baseline year was calculated as the average of 2008,
383 2009, 2010, 2013, and 2014. Geographically, the anomaly of all the four GPP products and
384 SIF showed very interesting spatial patterns at the seasonal and annual scales (Fig. 8).

385
386 **Figure 8 is here**

387 In the spring season, the middle and eastern CONUS experienced an increase in GPP
388 anomaly while western CONUS experienced a decrease, which was consistent with the
389 spatial pattern of SIF anomaly (Fig. 8a–e). The magnitudes and spatial extent of GPP
390 anomaly vary among the four GPP models. For GPP_{VPM} and GPP_{MOD17} , the large increases in
391 GPP (larger than $100 \text{ g C m}^{-2} \text{ season}^{-1}$) occurred mostly in the Southern Great Plains and part
392 of the Midwestern corn-belt region. For GPP_{CASA} , large increases in GPP occurred mostly in

393 the Midwestern and Southeast regions. The correlation analyses between GPP products and
394 SIF (Fig. 9a–d) showed that GPP_{VPM} and SIF had the strongest linear relationship ($R^2 = 0.67$),
395 followed by SIF/GPP_{MOD17} ($R^2 = 0.58$), SIF/GPP_{CASA} ($R^2 = 0.56$), and $SIF/GPP_{SiBCASA}$ ($R^2 =$
396 0.48).

397 **Table 2 is here**

398
399 In the summer season, most regions in CONUS experienced decreased GPP and SIF
400 associated with drought (Fig. 8f–j). The Great Plains and Midwestern corn-belt regions
401 experienced the largest reductions in GPP (larger than $150 \text{ g C m}^{-2} \text{ season}^{-1}$). The spatial
402 extents of decreased GPP in GPP_{VPM} and GPP_{MOD17} were greater than those in $GPP_{SiBCASA}$
403 and GPP_{CASA} . GPP_{VPM} , GPP_{CASA} , and $GPP_{SiBCASA}$ displayed strong increases in the southeast
404 regions, which was consistent with the spatial pattern of SIF anomaly. Overall, GPP_{VPM}
405 agreed best with SIF ($R^2 = 0.71$), followed by SIF/GPP_{CASA} ($R^2 = 0.50$), SIF/GPP_{MOD17} and
406 R^2 of 0.45), and $SIF/GPP_{SiBCASA}$ ($R^2 = 0.19$) (Fig. 9e–h).

407 **Figure 9 is here**

408
409 For the entire year, annual GPP_{VPM} , GPP_{MOD17} , and $GPP_{SiBCASA}$ mainly decreased in
410 the western US and corn-belt regions, and annual GPP increased mainly in the eastern and
411 southern forest area, which was consistent with the spatial pattern of SIF (Fig. 8k–o). Only
412 GPP_{CASA} reported strong increases in GPP in the corn-belt region. The correlation analysis
413 showed that none of the four GPP products agreed well with the spatial pattern of annual
414 mean SIF anomaly at the annual scale, with R^2 values varying from 0.14 to 0.27 (Fig. 9i–l).

415 When aggregated over the entire CONUS by season, the four GPP products and SIF clearly
416 showed an increase in GPP in the spring and a reduction in the summer, indicating the warm
417 spring and droughty summer had opposite effects on GPP (Fig. 8 and Table 2). The spring
418 warming led to an increase in GPP by 0.25-0.48 Pg C season⁻¹, where GPP_{CASA} showed the
419 largest increase and GPP_{SiBCASA} showed the least. During the summer, the four GPP products
420 showed a decrease in GPP by 0.21-0.42 Pg C season⁻¹, where GPP_{CASA} decreased the most
421 and GPP_{SiBCASA} decreased the least. The annual total GPP_{VPM} and GPP_{CASA} had an increase
422 of 0.11 and 0.18 Pg C year⁻¹, while the annual total GPP_{MOD17} and mean SIF had a
423 decrease of 0.12 Pg C year⁻¹ and 0.12 mW m⁻² nm⁻¹ sr⁻¹. The annual total GPP_{SiBCASA}
424 remained neutral in 2012.

425 **3.4 Impacts of spring warming and summer drought on GPP by biomes in 2012**

426 To quantify the impact of spring warming and summer drought on GPP across biomes,
427 we calculated total GPP from the four models for the four main biomes. In the spring of 2012,
428 all four models showed increased GPP for the four biomes (Fig. 10 and Table 3), and the
429 non-forest experienced a stronger increase in GPP than forest. In the four models, CASA
430 showed a larger increase in GPP in the spring than other three models in the four biomes,
431 while SiBCASA showed the lowest increase in GPP over most biomes. For the drought
432 summer, all four models showed strong decreases in GPP, and the grassland and cropland
433 experienced the strongest decrease, followed by other biomes. Among the four models,
434 MOD17 showed the largest decrease in GPP in the summer, while SiBCASA showed the
435 least decrease. For the entire year, grassland and cropland experienced a decrease in GPP,
436 while forest and other biomes experienced an increase or no change.

437

Figure 10 and Table 3 are here

438

439 4. Discussion

440 4.1 Improving GPP estimates of C₃ and C₄ croplands

441 Accurate estimation of cropland GPP is important for food production and security.
442 The MOD17 GPP data products have been widely used for crop studies (Guan et al. 2016;
443 Xin et al. 2015). However, several studies have reported that the MOD17 data product
444 substantially underestimates GPP in croplands. One reason is that ϵ_{max} for croplands in the
445 MOD17 model is too low (~ 1.04 g C MJ⁻¹) (Turner et al. 2006; Wagle et al. 2016; Xin et al.
446 2015). Site-level studies have indicated that the typical ϵ_{max} for C₃ crops range from 1.43 to
447 1.96 g C MJ⁻¹ (Chen et al. 2011; Kalfas et al. 2011; Yuan et al. 2015), and ϵ_{max} for C₄ crops
448 range from 2.25 to 4.06 g C MJ⁻¹ (Xin et al. 2015; Yuan et al. 2015). Several model
449 comparison studies have also showed that both process-based GPP models and LUE models
450 have poor performance when estimating GPP in croplands (Schaefer et al. 2012; Verma et al.
451 2014). Recently, Guanter et al. (2014) used GOME-2 SIF to estimate GPP in croplands using
452 the linear relationship between SIF and tower-based GPP at flux tower sites, and they found
453 these SIF-based GPP estimates in croplands were 50-60% higher than GPP estimates from
454 the ecosystem models over the US Corn Belt. In this study, our ϵ_{max} values for C₃ croplands
455 (1.80 g C MJ⁻¹) and C₄ croplands (2.7 g C MJ⁻¹) were based on previous site-level studies (Li
456 et al. 2013; Xin et al. 2015). The improved ability of VPM to capture the seasonal dynamics
457 and interannual variability of croplands was partly attributed to more appropriate choices of
458 ϵ_{max} values.

459 Another reason for the large error in estimating cropland GPP by the MOD17 and
460 other models can be attributed to the fact that we have very limited knowledge on the spatial
461 distribution of the C₃ and C₄ croplands within individual 500-m MODIS pixels and their

462 temporal dynamics over years (Reeves et al. 2005; Still et al. 2003; Wang et al. 2013).

463 However, in this study we used the fine-resolution, annual CDL cropland maps. The results

464 demonstrated the potential of annual C₃/C₄ cropland maps at high spatial resolution to

465 improve cropland GPP estimates from the individual pixel to country-wide scales. Although

466 there are several existing global C₃/C₄ maps, they are relatively coarse in spatial resolution

467 and produced only for a specific year. An early study developed a static C₃/C₄ fraction map

468 with a spatial resolution of 1°×1° by defining the favorable climate zones for C₃/C₄ and

469 combing the global spatial distribution of crop fractions and national harvest area data for

470 major crop types (Still et al. 2003). Another study developed a global distribution map of

471 croplands and pastures at a 5 min by 5 min (~10 km) spatial resolution in 2000 by combining

472 agricultural inventory data and satellite-derived land cover data (Ramankutty et al. 2008).

473 Recently, several studies made very limited progress in mapping C₃ and C₄ plants (both

474 croplands and grasses) when using remote sensing data and simple algorithms (Foody and

475 Dash 2007; Wang et al. 2013). The development of CDL datasets include the use of satellite-

476 based imagery, supervised image classification methodology, and numerous high-quality

477 ground truth data collected to help determine the multi-spectral rules from time-series

478 imagery that best predicted the land cover category. For grasslands, it was reported that there

479 was a strong linear relationship between the percentage of C₃ grass and the season-long

480 cumulative vegetation index (Foody and Dash 2007). These phenological features and time-

481 series MODIS data were used to classify C₃ and C₄ grasslands in the Great Plains (Wang et al.

482 2013). Given the importance of C₃ and C₄ plant function types in estimating GPP, it is

483 important for the remote sensing community to increase its effort in mapping C₃ and C₄

484 croplands and grasslands at site, regional, and global scales.

485 **4.2 The timing and location of climate extremes and their impacts on terrestrial**
486 **ecosystems**

487 Climate extremes such as heatwaves and droughts can reduce vegetative growth,
488 trigger large-scale tree mortality, and turn terrestrial ecosystems from carbon sinks into
489 sources (Ciais et al. 2005; Yuan et al. 2016). The warm spring and hot and dry summer in
490 2012 over CONUS offered a unique opportunity to investigate several major questions on the
491 impacts of climate extremes on terrestrial carbon cycle at the regional and continental scales
492 (He et al. 2018; Sippel et al. 2016; Wolf et al. 2016). Many studies have reported that
493 terrestrial ecosystems in CONUS have served as carbon sinks in recent decades (Hurtt et al.
494 2002; Pacala et al. 2001), ranging from 0.30 to 0.58 Pg C per year during the 1980s and
495 1990s, which accounts for 30% of fossil-fuel emissions from the USA. Wolf et al. (2016)
496 analyzed MOD17 GPP data and NEP data from CTE2014 during 2001–2012 and reported
497 that the increase of NEP in the spring compensated for the loss of NEP in the summer, which
498 resulted in a small carbon sink (0.11 Pg C year⁻¹ in 2012) for CONUS. This result suggests
499 the importance of assessing the impacts of climate extremes, which depend on timing,
500 duration, and location, on terrestrial carbon budgets at the annual and continental scales
501 (Sippel et al. 2017; von Buttlar et al. 2017).

502 Wolf et al. (2016) analyzed MOD17 GPP data in 2001–2012 and reported that GPP
503 loss in summer in 2012 over CONUS was twice as large as the increase in GPP in the spring
504 of 2012, resulting in a large annual loss of GPP (-0.38 Pg C). Though we used a different
505 baseline, our analysis of MOD17 GPP data in 2008–2014 also shows that the decrease in
506 GPP in the summer of 2012 was substantially larger than the increase in GPP in the spring of
507 2012, resulting in large annual loss of GPP (-0.12 Pg C) (Fig. 8). However, the results from
508 GPP_{VPM} , $GPP_{SiBCASA}$, and GPP_{CASA} showed that the GPP increase in the spring is close or

509 slightly larger than GPP loss in the summer of 2012, the annual GPP anomaly ranging from
510 0.01 ($GPP_{SiBCASA}$), to 0.11 Pg C (GPP_{VPM}), to 0.18 Pg C (GPP_{CASA}), while the GOME-2 SIF
511 anomaly showed a decrease in 2012 (Fig. 7). The differences in modeling GPP responses to
512 spring warming and summer drought among these four models are likely to affect our
513 understanding of the responses of ecosystem respiration (ER) to spring warming and summer
514 drought. As NEP is the sum of GPP (carbon gains) and ER (carbon losses), the large decrease
515 in GPP (e.g., $-0.38 \text{ Pg C year}^{-1}$ in 2012, GPP_{MOD17}) from the previous study (Wolf et al. 2016)
516 implied a slightly larger decrease in ER, which could then result in a small carbon sink (0.11
517 Pg C year^{-1} in 2012). In addition, since CASA-GFED3 and SiBCASA-GFED4 are the
518 biosphere models used by CarbonTracker (CT2014) and CarbonTracker Europe (CTE2014)
519 to generate prior biosphere carbon fluxes, the spatial-temporal differences in GPP distribution,
520 magnitude, and anomaly from these two models are likely to affect CarbonTracker and
521 CarbonTracker Europe outputs. Previous studies have reported that atmospheric CO_2
522 inversions are sensitive to the land surface prior fluxes, especially at fine scales and the areas
523 with sparse or no available observations (Peylin et al. 2013; Zhu et al. 2014). Therefore,
524 methods to incorporate more reliable carbon flux estimates from atmospheric CO_2 inversions
525 is critically needed for us to better understand the terrestrial carbon cycle.

526 **4.3 Differential responses to climate extremes across biomes**

527 Numerous studies have reported the negative impacts of high temperature and
528 droughts on vegetation productivity (Ciais et al. 2005; Welp et al. 2007; Wolf et al. 2016;
529 Yuan et al. 2016). Short-term drought or heatwaves lead to stomatal closure, membrane
530 damage, and disruption of photosynthetic enzyme activities, all of which reduce GPP. If
531 plants experience continuous drought, they may respond to drought stress by structural or
532 physiological adjustments such as decreased leaf area index, changes in the root-shoot ratio,
533 or changes in leaf angle (Frank et al. 2015). But different species have adopted different

534 strategies to deal with water stress. These strategies can be broadly classified as dehydration
535 tolerance or dehydration avoidance (Bacelar et al. 2012). Plants with a dehydration tolerance
536 strategy usually grow rapidly when water is available but will senesce and/or become
537 dormant during drought. Plants with a dehydration avoidance strategy tend to grow more
538 slowly and maintain greenness during drought by increasing water extraction from the soils
539 and reducing water loss from transpiration. Our study showed that the impacts of spring
540 warming and summer drought on the change in GPP varied across biomes (Fig. 10). This
541 change was not only due to the characteristics (timing, magnitude) of the heatwaves and
542 drought at specific regions (Fig. 11), but also species-specific plant drought responses and
543 strategies (von Buttlar et al. 2017; Wolf et al. 2014). Our results show that grasslands
544 experienced the largest reduction in GPP while forests had the largest increase. This
545 difference may be explained by the observation that grasslands are drought sensitive, and
546 more susceptible to heatwaves and droughts as they have less accessibility to soil water
547 (shallow roots) and higher turn-over rates (Frank et al. 2015). Trees usually have deeper roots
548 and better access to soil water, thus forests are considered to be less affected by heatwaves
549 and drought (Frank et al. 2015; van der Molen et al. 2011; Zhang et al. 2016b). Grasslands
550 occur in the most severe drought-affected areas, while most forests are in the northwestern
551 and eastern part of CONUS, which were either not affected by the 2012 drought or were
552 classified as abnormally dry (D0) by the U.S. drought monitor (Fig. 11). Cropland systems
553 are different from natural systems by the frequent human intervention (for example, irrigation
554 or changing planting date). Consequently, the impacts of climate extremes on croplands are
555 expected to be highly modulated by human management (Lobell et al. 2012; van der Velde et
556 al. 2010). However, cropland over the Corn Belt, the most important crop area in the US, is
557 mainly rainfed (Leng et al. 2016), leading to a similar GPP response to drought for cropland
558 and grasslands.

559

Figure 11 is here

560 4.4 Uncertainties and remaining issues

561 The uncertainty of ecosystem models remains a challenge for carbon cycling research.
562 Extreme climate events were found to dominate the global interannual variability of GPP
563 (Zscheischler et al. 2014). At present, most ecological models do not accurately represent the
564 responses of major ecosystem processes to climate extremes and do not accurately track the
565 interannual variability of GPP (Reichstein et al. 2013). For example, previous studies
566 indicated that improving GPP estimates for most models requires better representation of
567 water stress effects on photosynthesis (Schaefer et al. 2012; Verma et al. 2014; Yuan et al.
568 2014). In this study, VPM, MOD17, and CASA are all light use efficiency models, but use
569 different water regulation scalars. VPM uses a water-related vegetation index (LSWI) as the
570 water constraint, MOD17 uses vapor pressure deficit (VPD), and CASA uses the
571 evapotranspiration supply/demand ratio (actual evapotranspiration/potential
572 evapotranspiration). LSWI is found to be a good indicator of soil moisture when taking all the
573 biomes into consideration (Zhang et al. 2015). However, it may not work well for forested
574 areas because of the lower spectral sensitivity to water stress (Sims et al. 2014). VPD
575 represents the impacts of atmospheric dryness on vegetation photosynthesis because stomatal
576 conductance changes with VPD. However, soil moisture also plays an important role in
577 regulating GPP by affecting leaf cell turgor pressure or stomatal conductance, thereby
578 directly affecting photosynthesis (Hashimoto et al. 2013; Leuning et al. 2005). The
579 evapotranspiration ratio requires well simulated hydrologic fluxes in soils where additional
580 information (e.g. soil texture, soil/rooting depth) is required. This information is usually not
581 easy to collect and comes with uncertainties. Therefore, more effort is needed to quantify the
582 model uncertainties and improve model structure.

583 Since SIF can be directly observed from space, has a very good relationship with GPP
584 ([Guanter et al. 2014](#); [Wagle et al. 2016](#); [Zhang et al. 2016a](#)), and is a good indicator of
585 agricultural drought ([Sun et al. 2015](#)), we used SIF as a reference to which we compared the
586 impacts of spring warming and summer droughts on vegetation photosynthesis. However, we
587 acknowledge that GOME-2 SIF has some uncertainties, especially in the western part of
588 CONUS (Fig. 6) due to the relatively large signal-to-noise ratio ([Zhang et al. 2016a](#)). SIF
589 retrievals from recently launched satellites (OCO-2, Sentinel-5 Precursor, and FLEX-
590 Fluorescence Explorer) with higher spatial resolutions and observations tailored for SIF may
591 improve our understanding of the impacts of climate extremes on vegetation.

592 In this study, we only considered the impacts of climates extremes on terrestrial
593 ecosystems within a year. However, droughts may affect terrestrial ecosystems across months
594 or even years, depending upon plant functional types ([Frank et al. 2015](#); [von Buttlar et al.](#)
595 [2017](#)). Extreme events could cause plant functional loss, changes in the community structure
596 of ecosystems, increased wildfires, and pest and pathogen outbreaks, all which may
597 necessitate a long recovery period ([van der Molen et al. 2011](#)). Further, species' response to
598 climate extremes vary widely, and some impacts could persist long after extreme events
599 ([Rammig et al. 2014](#)). Analysis of the responses of terrestrial ecosystems to climate extremes
600 should be conducted over the next few years.

601 **5. Conclusions**

602 The spring warming and summer drought of 2012 across CONUS had substantial
603 impacts on the terrestrial carbon cycle and offered a unique opportunity to investigate the
604 responses of photosynthesis (GPP) and respiration processes at large scales. We presented an
605 improved VPM model that incorporates C₃ and C₄ croplands and can better capture the
606 seasonal dynamics and interannual variation of GPP than the MOD17 product when these

607 models are compared to GPP_{EC} data from eddy covariance flux tower sites. Spatial-temporal
608 comparisons among GOME-2 SIF, GPP_{MOD17} , and GPP_{VPM} products during 2008–2014
609 showed strong consistency between GOME-2 SIF and GPP_{VPM} data products. Anomaly
610 analyses of (1) annual GPP from three other models (VPM, SiBCASA, and CASA) and (2)
611 GOME-2 SIF data between the baseline years (2008, 2009, 2010, 2013, 2014) and drought
612 year 2012 suggested that increased GPP during the warm spring compensated for decreased
613 GPP during the dry and hot summer, resulting in close to net neutral changes in annual GPP.
614 The results from this study clearly highlight the importance of assessing the impacts of co-
615 occurring climate extremes at seasonal and annual scales over large spatial domains. Our
616 results demonstrate the need to further improve GPP models, which could increase the
617 accuracy and reduce uncertainties in GPP estimates of terrestrial ecosystems.

618 **Acknowledgements**

619 This work used eddy covariance data acquired and shared by the FLUXNET
620 community, including these networks: AmeriFlux, AfriFlux, AsiaFlux, CarboAfrica,
621 CarboEuropeIP, CarboItaly, CarboMont, ChinaFlux, Fluxnet-Canada, GreenGrass, ICOS,
622 KoFlux, LBA, NECC, OzFlux-TERN, TCOS-Siberia, and TERENO and USCCC. The
623 FLUXNET eddy covariance data processing and harmonization was carried out by the ICOS
624 Ecosystem Thematic Center, AmeriFlux Management Project and Fluxdata project of
625 FLUXNET, with the support of CDIAC, and the OzFlux, ChinaFlux and AsiaFlux offices.
626 This study is partly supported by the research grants (Project No. 2013-69002-23146 and
627 2016-68002-24967) through the USDA National Institute for Food and Agriculture (NIFA), a
628 research grant (IIA-1301789) from the US National Science Foundation EPSCoR program,
629 and a research grant (Geostationary Carbon Cycle Observatory mission, 80LARC17C0001)
630 from NASA. We acknowledge Ivar R. van der Velde for providing the SiBCASA-GFED4
631 simulations, the monthly $1^\circ \times 1^\circ$ SiBCASA-GFED4 GPP data over CONUS from 2008-2014

632 used is available at (https://github.com/xiaocuiwu/SiBCASA_GPP_monthly_CONUS.git).

633 The CASA-GFED3 project (<https://nacp-files.nacarbon.org/nacp-kawa-01>) is supported by

634 the North American Carbon Program. The VPM model code and the aggregated 1°×1° VPM

635 GPP over CONUS from 2008-2014 are available at

636 (https://github.com/xiaocuiwu/GPP_VPM_C3C4_CONUS.git).

637

638 **References**

- 639 Bacelar, E.L.V.A., Moutinho-Pereira, J.M., Gonçalves, B.M.C., Brito, C.V.Q., Gomes-Laranjo, J.,
640 Ferreira, H.M.F., & Correia, C.M. (2012). Water Use Strategies of Plants Under Drought
641 Conditions. In: Aroca R. (eds) Plant Responses to Drought Stress. Springer, Berlin,
642 Heidelberg, doi: https://doi.org/10.1007/978-3-642-32653-0_6
- 643 Baldocchi, D.D., Xu, L.K., & Kiang, N. (2004). How plant functional-type, weather, seasonal
644 drought, and soil physical properties alter water and energy fluxes of an oak-grass savanna
645 and an annual grassland. *Agricultural and Forest Meteorology*, 123, 13-39
- 646 Beer, C., Reichstein, M., Tomelleri, E., Ciais, P., Jung, M., Carvalhais, N., Rodenbeck, C., Arain,
647 M.A., Baldocchi, D., Bonan, G.B., Bondeau, A., Cescatti, A., Lasslop, G., Lindroth, A.,
648 Lomas, M., Luyssaert, S., Margolis, H., Oleson, K.W., Rouspard, O., Veenendaal, E., Viovy,
649 N., Williams, C., Woodward, F.I., & Papale, D. (2010). Terrestrial Gross Carbon Dioxide
650 Uptake: Global Distribution and Covariation with Climate. *Science*, 329, 834-838
- 651 Boryan, C., Yang, Z., Mueller, R., & Craig, M. (2011). Monitoring US agriculture: the US
652 Department of Agriculture, National Agricultural Statistics Service, Cropland Data Layer
653 Program. *Geocarto International*, 26, 341-358
- 654 Cavanaugh, M.L., Kurc, S.A., & Scott, R.L. (2011). Evapotranspiration partitioning in semiarid
655 shrubland ecosystems: a two-site evaluation of soil moisture control on transpiration.
656 *Ecohydrology*, 4, 671-681
- 657 Chen, J.M. (1996). Optically-based methods for measuring seasonal variation of leaf area index in
658 boreal conifer stands. *Agricultural and Forest Meteorology*, 80, 135-163
- 659 Chen, T., van der Werf, G.R., Dolman, A.J., & Groenendijk, M. (2011). Evaluation of cropland
660 maximum light use efficiency using eddy flux measurements in North America and Europe.
661 *Geophysical Research Letters*, 38, L14707, doi: 10.1029/2011GL047533
- 662 Chu, H.S., Chen, J.Q., Gottgens, J.F., Ouyang, Z.T., John, R., Czajkowski, K., & Becker, R. (2014).
663 Net ecosystem methane and carbon dioxide exchanges in a Lake Erie coastal marsh and a
664 nearby cropland. *Journal of Geophysical Research-Biogeosciences*, 119, 722-740
- 665 Ciais, P., Reichstein, M., Viovy, N., Granier, A., Ogee, J., Allard, V., Aubinet, M., Buchmann, N.,
666 Bernhofer, C., Carrara, A., Chevallier, F., De Noblet, N., Friend, A.D., Friedlingstein, P.,
667 Grunwald, T., Heinesch, B., Keronen, P., Knohl, A., Krinner, G., Loustau, D., Manca, G.,
668 Matteucci, G., Miglietta, F., Ourcival, J.M., Papale, D., Pilegaard, K., Rambal, S., Seufert,
669 G., Soussana, J.F., Sanz, M.J., Schulze, E.D., Vesala, T., & Valentini, R. (2005). Europe-
670 wide reduction in primary productivity caused by the heat and drought in 2003. *Nature*, 437,
671 529-533

- 672 Collatz, G.J., Ribas-Carbo, M., & Berry, J.A. (1992). Coupled Photosynthesis-Stomatal
673 Conductance Model for Leaves of C4 Plants. *Australian Journal of Plant Physiology*, 19,
674 519-538
- 675 Cook, B.D., Davis, K.J., Wang, W.G., Desai, A., Berger, B.W., Teclaw, R.M., Martin, J.G., Bolstad,
676 P.V., Bakwin, P.S., Yi, C.X., & Heilman, W. (2004). Carbon exchange and venting
677 anomalies in an upland deciduous forest in northern Wisconsin, USA. *Agricultural and*
678 *Forest Meteorology*, 126, 271-295
- 679 Disney, M., Lewis, P., & Saich, P. (2006). 3D modelling of forest canopy structure for remote
680 sensing simulations in the optical and microwave domains. *Remote Sensing of Environment*,
681 100, 114-132
- 682 Dong, J.W., Xiao, X.M., Wagle, P., Zhang, G.L., Zhou, Y.T., Jin, C., Torn, M.S., Meyers, T.P.,
683 Suyker, A.E., Wang, J.B., Yan, H.M., Biradar, C., & Moore, B. (2015). Comparison of four
684 EVI-based models for estimating gross primary production of maize and soybean croplands
685 and tallgrass prairie under severe drought. *Remote Sensing of Environment*, 162, 154-168
- 686 Doughty, R., Xiao, X., Wu, X., Zhang, Y., Bajgain, R., Zhou, Y., Qin, Y., Zou, Z., McCarthy, H.,
687 Friedman, J., Wagle, P., Basara, J., & Steiner, J. (2018). Responses of gross primary
688 production of grasslands and croplands under drought, pluvial, and irrigation conditions
689 during 2010–2016, Oklahoma, USA. *Agricultural Water Management*, 204, 47-59
- 690 Farquhar, G.D., Caemmerer, S.V., & Berry, J.A. (1980). A Biochemical Model of Photosynthetic
691 CO₂ Assimilation in Leaves of C3 Species. *Planta*, 149, 78-90
- 692 Fischer, M.L., Billesbach, D.P., Berry, J.A., Riley, W.J., & Torn, M.S. (2007). Spatiotemporal
693 Variations in Growing Season Exchanges of CO₂, H₂O, and Sensible Heat in Agricultural
694 Fields of the Southern Great Plains. *Earth Interactions*, 11, 1-21
- 695 Foody, G.M., & Dash, J. (2007). Discriminating and mapping the C3 and C4 composition of
696 grasslands in the northern Great Plains, USA. *Ecological Informatics*, 2, 89-93
- 697 Frank, D., Reichstein, M., Bahn, M., Thonicke, K., Frank, D., Mahecha, M.D., Smith, P., van der
698 Velde, M., Vicca, S., Babst, F., Beer, C., Buchmann, N., Canadell, J.G., Ciais, P., Cramer,
699 W., Ibrom, A., Miglietta, F., Poulter, B., Rammig, A., Seneviratne, S.I., Walz, A.,
700 Wattenbach, M., Zavala, M.A., & Zscheischler, J. (2015). Effects of climate extremes on the
701 terrestrial carbon cycle: concepts, processes and potential future impacts. *Global Change*
702 *Biology*, 21, 2861-2880
- 703 Frankenberg, C., Fisher, J.B., Worden, J., Badgley, G., Saatchi, S.S., Lee, J.-E., Toon, G.C., Butz,
704 A., Jung, M., Kuze, A., & Yokota, T. (2011). New global observations of the terrestrial
705 carbon cycle from GOSAT: Patterns of plant fluorescence with gross primary productivity.
706 *Geophysical Research Letters*, 38, L17706, doi: 10.1029/2011GL048738
- 707 Friedl, M.A., Sulla-Menashe, D., Tan, B., Schneider, A., Ramankutty, N., Sibley, A., & Huang, X.
708 (2010). MODIS Collection 5 global land cover: Algorithm refinements and characterization
709 of new datasets. *Remote Sensing of Environment*, 114, 168-182
- 710 Gough, C.M., Hardiman, B.S., Nave, L.E., Bohrer, G., Maurer, K.D., Vogel, C.S., Nadelhoffer, K.J.,
711 & Curtis, P.S. (2013). Sustained carbon uptake and storage following moderate disturbance
712 in a Great Lakes forest. *Ecological Applications*, 23, 1202-1215
- 713 Gough, C.M., Vogel, C.S., Schmid, H.P., Su, H.B., & Curtis, P.S. (2008). Multi-year convergence
714 of biometric and meteorological estimates of forest carbon storage. *Agricultural and Forest*
715 *Meteorology*, 148, 158-170
- 716 Guan, K., Berry, J.A., Zhang, Y., Joiner, J., Guanter, L., Badgley, G., & Lobell, D.B. (2016).
717 Improving the monitoring of crop productivity using spaceborne solar-induced fluorescence.
718 *Global Change Biology*, 22, 716-726

- 719 Guanter, L., Zhang, Y., Jung, M., Joiner, J., Voigt, M., Berry, J.A., Frankenberg, C., Huete, A.R.,
720 Zarco-Tejada, P., Lee, J.E., Moran, M.S., Ponce-Campos, G., Beer, C., Camps-Valls, G.,
721 Buchmann, N., Gianelle, D., Klumpp, K., Cescatti, A., Baker, J.M., & Griffis, T.J. (2014).
722 Global and time-resolved monitoring of crop photosynthesis with chlorophyll fluorescence.
723 *Proceedings of the National Academy of Sciences of the United States of America*, *111*,
724 E1327-1333
- 725 Hashimoto, H., Wang, W., Milesi, C., Xiong, J., Ganguly, S., Zhu, Z., & Nemani, R. (2013).
726 Structural Uncertainty in Model-Simulated Trends of Global Gross Primary Production.
727 *Remote Sensing*, *5*, 1258-1273
- 728 Hatala, J.A., Detto, M., Sonnentag, O., Deverel, S.J., Verfaillie, J., & Baldocchi, D.D. (2012).
729 Greenhouse gas (CO₂, CH₄, H₂O) fluxes from drained and flooded agricultural peatlands in
730 the Sacramento-San Joaquin Delta. *Agriculture Ecosystems & Environment*, *150*, 1-18
- 731 He, W., Ju, W., Schwalm, C., Sippel, S., Wu, X., He, Q., Song, L., Zhang, C., Li, J., Sitch, S., Viovy,
732 N., Friedlingstein, P., & Jain, A. (2018). Terrestrial net carbon uptake over North America
733 in 2011 and 2012. *Journal of Geophysical Research-Biogeosciences*, *123*
- 734 Hilker, T., Lyapustin, A.I., Tucker, C.J., Hall, F.G., Myneni, R.B., Wang, Y.J., Bi, J., de Moura,
735 Y.M., & Sellers, P.J. (2014). Vegetation dynamics and rainfall sensitivity of the Amazon.
736 *Proceedings of the National Academy of Sciences of the United States of America*, *111*,
737 16041-16046
- 738 Hilton, T.W., Whelan, M.E., Zumkehr, A., Kulkarni, S., Berry, J.A., Baker, I.T., Montzka, S.A.,
739 Sweeney, C., Miller, B.R., & Elliott Campbell, J. (2017). Peak growing season gross uptake
740 of carbon in North America is largest in the Midwest USA. *Nature Climate Change*, *7*, 450-
741 454
- 742 Hoerling, M., Eischeid, J., Kumar, A., Leung, R., Mariotti, A., Mo, K., Schubert, S., & Seager, R.
743 (2014). Causes and Predictability of the 2012 Great Plains Drought. *Bulletin of the*
744 *American Meteorological Society*, *95*, 269-282
- 745 Huete, A.R., Liu, H.Q., Batchily, K., & vanLeeuwen, W. (1997). A comparison of vegetation
746 indices global set of TM images for EOS-MODIS. *Remote Sensing of Environment*, *59*,
747 440-451
- 748 Hurtt, G.C., Pacala, S.W., Moorcroft, P.R., Caspersen, J., Shevliakova, E., Houghton, R.A., &
749 Moore, B., 3rd (2002). Projecting the future of the U.S. carbon sink. *Proceedings of the*
750 *National Academy of Sciences of the United States of America*, *99*, 1389-1394
- 751 Jin, C., Xiao, X., Merbold, L., Arneith, A., Veenendaal, E., & Kutsch, W.L. (2013). Phenology and
752 gross primary production of two dominant savanna woodland ecosystems in Southern
753 Africa. *Remote Sensing of Environment*, *135*, 189-201
- 754 Jin, C., Xiao, X.M., Wagle, P., Griffis, T., Dong, J.W., Wu, C.Y., Qin, Y.W., & Cook, D.R. (2015).
755 Effects of in-situ and reanalysis climate data on estimation of cropland gross primary
756 production using the Vegetation Photosynthesis Model. *Agricultural and Forest*
757 *Meteorology*, *213*, 240-250
- 758 Joiner, J., Guanter, L., Lindstrot, R., Voigt, M., Vasilkov, A.P., Middleton, E.M., Huemmrich, K.F.,
759 Yoshida, Y., & Frankenberg, C. (2013). Global monitoring of terrestrial chlorophyll
760 fluorescence from moderate-spectral-resolution near-infrared satellite measurements:
761 methodology, simulations, and application to GOME-2. *Atmospheric Measurement*
762 *Techniques*, *6*, 2803-2823
- 763 Kalfas, J.L., Xiao, X., Vanegas, D.X., Verma, S.B., & Suyker, A.E. (2011). Modeling gross primary
764 production of irrigated and rain-fed maize using MODIS imagery and CO₂ flux tower data.
765 *Agricultural and Forest Meteorology*, *151*, 1514-1528

- 766 Knutson, T.R., Zeng, F., & Wittenberg, A.T. (2013). The extreme March-May 2012 warm anomaly
767 over the Eastern United States: Global context and multimodel trend analysis. *Bulletin of the*
768 *American Meteorological Society*, 94, S13-S17
- 769 Lasslop, G., Reichstein, M., Papale, D., Richardson, A.D., Arneth, A., Barr, A., Stoy, P., &
770 Wohlfahrt, G. (2010). Separation of net ecosystem exchange into assimilation and
771 respiration using a light response curve approach: critical issues and global evaluation.
772 *Global Change Biology*, 16, 187-208
- 773 Law, B.E., Turner, D., Campbell, J., Sun, O.J., Van Tuyl, S., Ritts, W.D., & Cohen, W.B. (2004).
774 Disturbance and climate effects on carbon stocks and fluxes across Western Oregon USA.
775 *Global Change Biology*, 10, 1429-1444
- 776 Law, B.E., Williams, M., Anthoni, P.M., Baldocchi, D., & Unsworth, M.H. (2000). Measuring and
777 modelling seasonal variation of carbon dioxide and water vapour exchange of a pinus
778 ponderosa forest subject to soil water deficit. *Global Change Biology*, 6, 613-630
- 779 Le Quéré, C., Raupach, M.R., Canadell, J.G., Marland, G., Le Quéré et al, C., Le Quéré et al, C.,
780 Raupach, M.R., Canadell, J.G., Marland, G., Bopp, L., Ciais, P., Conway, T.J., Doney, S.C.,
781 Feely, R.A., Foster, P., Friedlingstein, P., Gurney, K., Houghton, R.A., House, J.I.,
782 Huntingford, C., Levy, P.E., Lomas, M.R., Majkut, J., Metzl, N., Ometto, J.P., Peters, G.P.,
783 Prentice, I.C., Randerson, J.T., Running, S.W., Sarmiento, J.L., Schuster, U., Sitch, S.,
784 Takahashi, T., Viovy, N., van der Werf, G.R., Woodward, F.I., & et al. (2009). Trends in the
785 sources and sinks of carbon dioxide. *Nature Geoscience*, 2, 831-836
- 786 Leng, G.Y., Zhang, X.S., Huang, M.Y., Yang, Q.C., Rafique, R., Asrar, G.R., & Leung, L.R. (2016).
787 Simulating county-level crop yields in the Conterminous United States using the
788 Community Land Model: The effects of optimizing irrigation and fertilization. *Journal of*
789 *Advances in Modeling Earth Systems*, 8, 1912-1931
- 790 Leuning, R., Cleugh, H.A., Zegelin, S.J., & Hughes, D. (2005). Carbon and water fluxes over a
791 temperate Eucalyptus forest and a tropical wet/dry savanna in Australia: measurements and
792 comparison with MODIS remote sensing estimates. *Agricultural and Forest Meteorology*,
793 129, 151-173
- 794 Li, X.L., Liang, S.L., Yu, G.R., Yuan, W.P., Cheng, X., Xia, J.Z., Zhao, T.B., Feng, J.M., Ma, Z.G.,
795 Ma, M.G., Liu, S.M., Chen, J.Q., Shao, C.L., Li, S.G., Zhang, X.D., Zhang, Z.Q., Chen, S.P.,
796 Ohta, T., Varlagin, A., Miyata, A., Takagi, K., Saiqusa, N., & Kato, T. (2013). Estimation of
797 gross primary production over the terrestrial ecosystems in China. *Ecological Modelling*,
798 261, 80-92
- 799 Lobell, D.B., Hicke, J.A., Asner, G.P., Field, C., Tucker, C., & Los, S. (2002). Satellite estimates of
800 productivity and light use efficiency in United States agriculture, 1982-98. *Global Change*
801 *Biology*, 8, 722-735
- 802 Lobell, D.B., Sibley, A., & Ivan Ortiz-Monasterio, J. (2012). Extreme heat effects on wheat
803 senescence in India. *Nature Climate Change*, 2, 186-189
- 804 Ma, S., Baldocchi, D.D., Xu, L., & Hehn, T. (2007). Inter-annual variability in carbon dioxide
805 exchange of an oak/grass savanna and open grassland in California. *Agricultural and Forest*
806 *Meteorology*, 147, 157-171
- 807 Matamala, R., Jastrow, J.D., Miller, R.M., & Garten, C.T. (2008). Temporal changes in C and N
808 stocks of restored prairie: Implications for C sequestration strategies. *Ecological*
809 *Applications*, 18, 1470-1488
- 810 Monteith, J.L. (1972). Solar-Radiation and Productivity in Tropical Ecosystems. *Journal of Applied*
811 *Ecology*, 9, 747-766
- 812 Monteith, J.L. (1977). Climate and Efficiency of Crop Production in Britain. *Philosophical*
813 *Transactions of the Royal Society of London Series B-Biological Sciences*, 281, 277-294

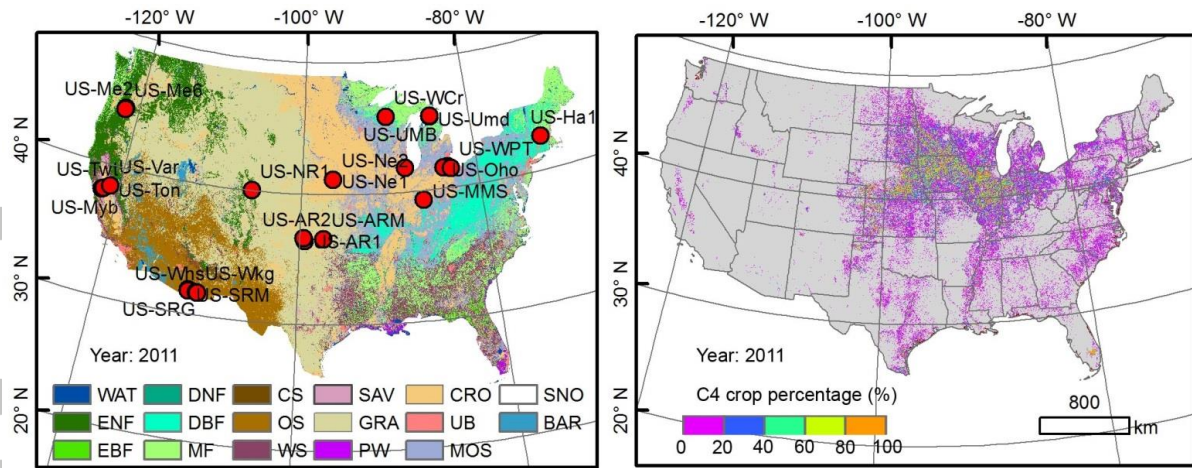
- 814 Ollinger, S.V. (2011). Sources of variability in canopy reflectance and the convergent properties of
815 plants. *New Phytologist*, 189, 375-394
- 816 Pacala, S., Hurtt, G., Baker, D.B., & Peylin, P. (2001). Consistent land- and atmosphere-based U.S.
817 carbon sink estimates. *Science*, 292, 2316-2319
- 818 Pan, Y.D., & Schimel, D. (2016). Biogeochemistry: Synergy of a warm spring and dry summer.
819 *Nature*, 534, 483-484
- 820 Parazoo, N.C., Barnes, E., Worden, J., Harper, A.B., Bowman, K.B., Frankenberg, C., Wolf, S.,
821 Litvak, M., & Keenan, T.F. (2015). Influence of ENSO and the NAO on terrestrial carbon
822 uptake in the Texas-northern Mexico region. *Global Biogeochemical Cycles*, 29, 1247-1265
- 823 Peters, W., Jacobson, A.R., Sweeney, C., Andrews, A.E., Conway, T.J., Masarie, K., Miller, J.B.,
824 Bruhwiler, L.M., Petron, G., Hirsch, A.I., Worthy, D.E., van der Werf, G.R., Randerson,
825 J.T., Wennberg, P.O., Krol, M.C., & Tans, P.P. (2007). An atmospheric perspective on
826 North American carbon dioxide exchange: CarbonTracker. *Proceedings of the National
827 Academy of Sciences of the the United States of America*, 104, 18925-18930
- 828 Peylin, P., Law, R.M., Gurney, K.R., Chevallier, F., Jacobson, A.R., Maki, T., Niwa, Y., Patra, P.K.,
829 Peters, W., Rayner, P.J., Rödenbeck, C., van der Laan-Luijkx, I.T., & Zhang, X. (2013).
830 Global atmospheric carbon budget: results from an ensemble of atmospheric CO₂ inversions.
831 *Biogeosciences*, 10, 6699-6720
- 832 Porcar-Castell, A., Tyystjarvi, E., Atherton, J., van der Tol, C., Flexas, J., Pfundel, E.E., Moreno, J.,
833 Frankenberg, C., & Berry, J.A. (2014). Linking chlorophyll a fluorescence to photosynthesis
834 for remote sensing applications: mechanisms and challenges. *Journal of Experimental
835 Botany*, 65, 4065-4095
- 836 Potter, C., Klooster, S., Genovese, V., Hiatt, C., Boriah, S., Kumar, V., Mithal, V., & Garg, A.
837 (2012). Terrestrial ecosystem carbon fluxes predicted from MODIS satellite data and large-
838 scale disturbance modeling. *International Journal of Geosciences*, 3(03), 469-479
- 839 Potter, C., Randerson, J.T., Field, C., Matson, P., Vitousek, P., Mooney, H., & Klooster, S. (1993).
840 Terrestrial ecosystem production: A process model based on global satellite and surface data.
841 *Global Biogeochemical Cycles*, 7, 811-841
- 842 Ramankutty, N., Evan, A.T., Monfreda, C., & Foley, J.A. (2008). Farming the planet: 1. Geographic
843 distribution of global agricultural lands in the year 2000. *Global Biogeochemical Cycles*, 22,
844 GB1003, doi: 10.1029/2007GB002953
- 845 Rammig, A., Wiedermann, M., Donges, J.F., Babst, F., von Bloh, W., Frank, D., Thonicke, K., &
846 Mahecha, M.D. (2014). Tree-ring responses to extreme climate events as benchmarks for
847 terrestrial dynamic vegetation models. *Biogeosciences Discussions*, 11, 2537-2568
- 848 Randerson, J.T., Thompson, M.V., Malmstrom, C.M., Field, C.B., & Fung, I.Y. (1996). Substrate
849 limitations for heterotrophs: Implications for models that estimate the seasonal cycle of
850 atmospheric CO₂. *Global Biogeochemical Cycles*, 10, 585-602
- 851 Reeves, M.C., Zhao, M., & Running, S.W. (2005). Usefulness and limits of MODIS GPP for
852 estimating wheat yield. *International Journal of Remote Sensing*, 26, 1403-1421
- 853 Reichstein, M., Bahn, M., Ciais, P., Frank, D., Mahecha, M.D., Seneviratne, S.I., Zscheischler, J.,
854 Beer, C., Buchmann, N., Frank, D.C., Papale, D., Rammig, A., Smith, P., Thonicke, K., van
855 der Velde, M., Vicca, S., Walz, A., & Wattenbach, M. (2013). Climate extremes and the
856 carbon cycle. *Nature*, 500, 287-295
- 857 Reichstein, M., Ciais, P., Papale, D., Valentini, R., Running, S., Viovy, N., Cramer, W., Granier, A.,
858 OgÉE, J., Allard, V., Aubinet, M., Bernhofer, C., Buchmann, N., Carrara, A., GrÜNwald, T.,
859 Heimann, M., Heinesch, B., Knohl, A., Kutsch, W., Loustau, D., Manca, G., Matteucci, G.,
860 Miglietta, F., Ourcival, J.M., Pilegaard, K., Pumpanen, J., Rambal, S., Schaphoff, S., Seufert,
861 G., Soussana, J.F., Sanz, M.J., Vesala, T., & Zhao, M. (2007). Reduction of ecosystem

- 862 productivity and respiration during the European summer 2003 climate anomaly: a joint flux
863 tower, remote sensing and modelling analysis. *Global Change Biology*, *13*, 634-651
- 864 Reichstein, M., Falge, E., Baldocchi, D., Papale, D., Aubinet, M., Berbigier, P., Bernhofer, C.,
865 Buchmann, N., Gilmanov, T., Granier, A., Grunwald, T., Havrankova, K., Ilvesniemi, H.,
866 Janous, D., Knohl, A., Laurila, T., Lohila, A., Loustau, D., Matteucci, G., Meyers, T.,
867 Miglietta, F., Ourcival, J.-M., Pumpanen, J., Rambal, S., Rotenberg, E., Sanz, M., Tenhunen,
868 J., Seufert, G., Vaccari, F., Vesala, T., Yakir, D., & Valentini, R. (2005). On the separation
869 of net ecosystem exchange into assimilation and ecosystem respiration: review and
870 improved algorithm. *Global Change Biology*, *11*, 1424-1439
- 871 Rippey, B.R. (2015). The U.S. drought of 2012. *Weather and Climate Extremes*, *10*, Part A, 57-64
- 872 Running, S., Nemani, R., Heinsch, F.A., Zhao, M., Reeves, M., & Hashimoto, H. (2004). A
873 contiguous satellite-derived measure of global terrestrial primary production. *Bioscience*, *54*,
874 547-560
- 875 Schaefer, K., Collatz, G.J., Tans, P., Denning, A.S., Baker, I., Berry, J., Prihodko, L., Suits, N., &
876 Philpott, A. (2008). Combined Simple Biosphere/Carnegie-Ames-Stanford Approach
877 terrestrial carbon cycle model. *Journal of Geophysical Research*, *113*, G03034, doi:
878 10.1029/2007JG000603
- 879 Schaefer, K., Schwalm, C.R., Williams, C., Arain, M.A., Barr, A., Chen, J.M., Davis, K.J., Dimitrov,
880 D., Hilton, T.W., Hollinger, D.Y., Humphreys, E., Poulter, B., Raczka, B.M., Richardson,
881 A.D., Sahoo, A., Thornton, P., Vargas, R., Verbeeck, H., Anderson, R., Baker, I., Black,
882 T.A., Bolstad, P., Chen, J., Curtis, P.S., Desai, A.R., Dietze, M., Dragoni, D., Gough, C.,
883 Grant, R.F., Gu, L., Jain, A., Kucharik, C., Law, B., Liu, S., Lokipitiya, E., Margolis, H.A.,
884 Matamala, R., McCaughey, J.H., Monson, R., Munger, J.W., Oechel, W., Peng, C., Price,
885 D.T., Ricciuto, D., Riley, W.J., Roulet, N., Tian, H., Tonitto, C., Torn, M., Weng, E., &
886 Zhou, X. (2012). A model-data comparison of gross primary productivity: Results from the
887 North American Carbon Program site synthesis. *Journal of Geophysical Research:*
888 *Biogeosciences*, *117*, doi:10.1029/2007JG000603
- 889 Schmid, H.P., Grimmond, S.B., Cropley, F., Offerle, B., & Su, H. (2000). Measurements of CO₂
890 and energy fluxes over a mixed hardwood forest in the mid-western United States.
891 *Agricultural and Forest Meteorology*, *103*, 357-374
- 892 Schwalm, C.R., Williams, C.A., Schaefer, K., Anderson, R., Arain, M.A., Baker, I., Barr, A., Black,
893 T.A., Chen, G., Chen, J.M., Ciais, P., Davis, K.J., Desai, A., Dietze, M., Dragoni, D.,
894 Fischer, M.L., Flanagan, L.B., Grant, R., Gu, L., Hollinger, D., Izaurralde, R.C., Kucharik,
895 C., Lafleur, P., Law, B.E., Li, L., Li, Z., Liu, S., Lokupitiya, E., Luo, Y., Ma, S., Margolis,
896 H., Matamala, R., McCaughey, H., Monson, R.K., Oechel, W.C., Peng, C., Poulter, B.,
897 Price, D.T., Ricciutto, D.M., Riley, W., Sahoo, A.K., Sprintsin, M., Sun, J., Tian, H., Tonitto,
898 C., Verbeeck, H., & Verma, S.B. (2010). A model-data intercomparison of CO₂ exchange
899 across North America: Results from the North American Carbon Program site synthesis.
900 *Journal of Geophysical Research*, *115*, doi: 10.1029/2009JG001229
- 901 Scott, R.L., Biederman, J.A., Hamerlynck, E.P., & Barron-Gafford, G.A. (2015). The carbon
902 balance pivot point of southwestern U.S. semiarid ecosystems: Insights from the 21st
903 century drought. *Journal of Geophysical Research: Biogeosciences*, *120*, 2612-2624
- 904 Scott, R.L., Hamerlynck, E.P., Jenerette, G.D., Moran, M.S., & Barron-Gafford, G.A. (2010).
905 Carbon dioxide exchange in a semidesert grassland through drought-induced vegetation
906 change. *Journal of Geophysical Research*, *115*, doi:10.1029/2010JG001348
- 907 Scott, R.L., Jenerette, G.D., Potts, D.L., & Huxman, T.E. (2009). Effects of seasonal drought on net
908 carbon dioxide exchange from a woody-plant-encroached semiarid grassland. *Journal of*
909 *Geophysical Research*, *114*, doi:10.1029/2008JG000900

- 910 Sims, D.A., Brzostek, E.R., Rahman, A.F., Dragoni, D., & Phillips, R.P. (2014). An improved
911 approach for remotely sensing water stress impacts on forest C uptake. *Global Change*
912 *Biology*, 20, 2856-2866
- 913 Sippel, S., Forkel, M., Rammig, A., Thonicke, K., Flach, M., Heimann, M., Otto, F.E.L., Reichstein,
914 M., & Mahecha, M.D. (2017). Contrasting and interacting changes in simulated spring and
915 summer carbon cycle extremes in European ecosystems. *Environmental Research Letters*,
916 12, 075006
- 917 Sippel, S., Zscheischler, J., & Reichstein, M. (2016). Ecosystem impacts of climate extremes
918 crucially depend on the timing. *Proceedings of the National Academy of Sciences of the*
919 *United States of America*, 113, 5768-5770
- 920 Still, C.J., Berry, J.A., Collatz, G.J., & DeFries, R.S. (2003). Global distribution of C₃ and C₄
921 vegetation: carbon cycle implications. *Global Biogeochemical Cycles*, 17, 1006, doi:
922 10.1029/2001GB001807
- 923 Sturtevant, C., Ruddell, B.L., Knox, S.H., Verfaillie, J., Matthes, J.H., Oikawa, P.Y., & Baldocchi,
924 D. (2016). Identifying scale-emergent, nonlinear, asynchronous processes of wetland
925 methane exchange. *Journal of Geophysical Research-Biogeosciences*, 121, 188-204
- 926 Sun, Y., Frankenberg, C., Wood, J.D., Schimel, D.S., Jung, M., Guanter, L., Drewry, D.T., Verma,
927 M., Porcar-Castell, A., Griffis, T.J., Gu, L., Magney, T.S., Kohler, P., Evans, B., & Yuen, K.
928 (2017). OCO-2 advances photosynthesis observation from space via solar-induced
929 chlorophyll fluorescence. *Science*, 358, eaam5747, doi: 10.1126/science.aam5747
- 930 Sun, Y., Fu, R., Dickinson, R., Joiner, J., Frankenberg, C., Gu, L.H., Xia, Y.L., & Fernando, N.
931 (2015). Drought onset mechanisms revealed by satellite solar-induced chlorophyll
932 fluorescence: Insights from two contrasting extreme events. *Journal of Geophysical*
933 *Research-Biogeosciences*, 120, 2427-2440,
- 934 Suyker, A.E., Verma, S.B., Burba, G.G., & Arkebauer, T.J. (2005). Gross primary production and
935 ecosystem respiration of irrigated maize and irrigated soybean during a growing season.
936 *Agricultural and Forest Meteorology*, 131, 180-190
- 937 Turner, D.P., Ritts, W.D., Cohen, W.B., Gower, S.T., Running, S.W., Zhao, M., Costa, M.H.,
938 Kirschbaum, A.A., Ham, J.M., Saleska, S.R., & Ahl, D.E. (2006). Evaluation of MODIS
939 NPP and GPP products across multiple biomes. *Remote Sensing of Environment*, 102, 282-
940 292
- 941 Urbanski, S., Barford, C., Wofsy, S., Kucharik, C., Pyle, E., Budney, J., McKain, K., Fitzjarrald, D.,
942 Czikowsky, M., & Munger, J.W. (2007). Factors controlling CO₂ exchange on timescales
943 from hourly to decadal at Harvard Forest. *Journal of Geophysical Research*, 112, doi:
944 10.1029/2006JG000293
- 945 van der Laan-Luijkx, I.T., van der Velde, I.R., van der Veen, E., Tsuruta, A., Stanislawska, K.,
946 Babenhauserheide, A., Zhang, H.F., Liu, Y., He, W., Chen, H., Masarie, K.A., Krol, M.C.,
947 & Peters, W. (2017). The CarbonTracker Data Assimilation Shell (CTDAS) v1.0:
948 implementation and global carbon balance 2001–2015. *Geoscientific Model Development*,
949 10, 2785-2800
- 950 van der Molen, M.K., Dolman, A.J., Ciais, P., Eglin, T., Gobron, N., Law, B.E., Meir, P., Peters, W.,
951 Phillips, O.L., Reichstein, M., Chen, T., Dekker, S.C., Doubkova, M., Friedl, M.A., Jung,
952 M., van den Hurk, B.J.J.M., de Jeu, R.A.M., Kruijt, B., Ohta, T., Rebel, K.T., Plummer, S.,
953 Seneviratne, S.I., Sitch, S., Teuling, A.J., van der Werf, G.R., & Wang, G. (2011). Drought
954 and ecosystem carbon cycling. *Agricultural and Forest Meteorology*, 151, 765-773
- 955 van der Velde, I.R., Miller, J.B., Schaefer, K., van der Werf, G.R., Krol, M.C., & Peters, W. (2014).
956 Terrestrial cycling of 13CO₂ by photosynthesis, respiration, and biomass burning in
957 SiBCASA. *Biogeosciences*, 11, 6553-6571

- 958 van der Velde, M., Wriedt, G., & Bouraoui, F. (2010). Estimating irrigation use and effects on maize
959 yield during the 2003 heatwave in France☆. *Agriculture, Ecosystems & Environment*, *135*,
960 90-97
- 961 van der Werf, G.R., Randerson, J.T., Giglio, L., Collatz, G.J., Kasibhatla, P.S., & Arellano, A.F.
962 (2006). Interannual variability in global biomass burning emissions from 1997 to 2004.
963 *Atmospheric Chemistry and Physics*, *6*, 3423-3441
- 964 van der Werf, G.R., Randerson, J.T., Giglio, L., Collatz, G.J., Mu, M., Kasibhatla, P.S., Morton,
965 D.C., DeFries, R.S., Jin, Y., & van Leeuwen, T.T. (2010). Global fire emissions and the
966 contribution of deforestation, savanna, forest, agricultural, and peat fires (1997-2009).
967 *Atmospheric Chemistry and Physics*, *10*, 11707-11735
- 968 van Gorsel, E., Delpierre, N., Leuning, R., Black, A., Munger, J.W., Wofsy, S., Aubinet, M.,
969 Feigenwinter, C., Beringer, J., Bonal, D., Chen, B., Chen, J., Clement, R., Davis, K.J., Desai,
970 A.R., Dragoni, D., Etzold, S., Grünwald, T., Gu, L., Heinesch, B., Hutyra, L.R., Jans,
971 W.W.P., Kutsch, W., Law, B.E., Leclerc, M.Y., Mammarella, I., Montagnani, L., Noormets,
972 A., Rebmann, C., & Wharton, S. (2009). Estimating nocturnal ecosystem respiration from
973 the vertical turbulent flux and change in storage of CO₂. *Agricultural and Forest*
974 *Meteorology*, *149*, 1919-1930
- 975 Verma, M., Friedl, M.A., Richardson, A.D., Kiely, G., Cescatti, A., Law, B.E., Wohlfahrt, G.,
976 Gielen, B., Roupsard, O., Moors, E.J., Toscano, P., Vaccari, F.P., Gianelle, D., Bohrer, G.,
977 Varlagin, A., Buchmann, N., van Gorsel, E., Montagnani, L., & Propastin, P. (2014).
978 Remote sensing of annual terrestrial gross primary productivity from MODIS: an
979 assessment using the FLUXNET La Thuile data set. *Biogeosciences*, *11*, 2185-2200
- 980 von Buttlar, J., Zscheischler, J., Rammig, A., Sippel, S., Reichstein, M., Knohl, A., Jung, M.,
981 Menzer, O., Arain, M.A., Buchmann, N., Cescatti, A., Gianelle, D., Kieley, G., Law, B.E.,
982 Magliulo, V., Margolis, H., McCaughey, H., Merbold, L., Migliavacca, M., Montagnani, L.,
983 Oechel, W., Pavelka, M., Peichl, M., Rambal, S., Raschi, A., Scott, R.L., Vaccari, F.P., van
984 Gorsel, E., Varlagin, A., Wohlfahrt, G., & Mahecha, M.D. (2017). Impacts of droughts and
985 extreme temperature events on gross primary production and ecosystem respiration: a
986 systematic assessment across ecosystems and climate zones. *Biogeosciences Discussions*, *1*-
987 39
- 988 Wagle, P., Xiao, X.M., & Suyker, A.E. (2015). Estimation and analysis of gross primary production
989 of soybean under various management practices and drought conditions. *Isprs Journal of*
990 *Photogrammetry and Remote Sensing*, *99*, 70-83
- 991 Wagle, P., Zhang, Y.G., Jin, C., & Xiao, X.M. (2016). Comparison of solar-induced chlorophyll
992 fluorescence, light-use efficiency, and process-based GPP models in maize. *Ecological*
993 *Applications*, *26*, 1211-1222
- 994 Wang, C., Hunt, E.R., Zhang, L., & Guo, H.D. (2013). Phenology-assisted classification of C3 and
995 C4 grasses in the U.S. Great Plains and their climate dependency with MODIS time series.
996 *Remote Sensing of Environment*, *138*, 90-101
- 997 Welp, L.R., Randerson, J.T., & Liu, H.P. (2007). The sensitivity of carbon fluxes to spring warming
998 and summer drought depends on plant functional type in boreal forest ecosystems.
999 *Agricultural and Forest Meteorology*, *147*, 172-185
- 1000 Wolf, S., Eugster, W., Ammann, C., Häni, M., Zielis, S., Hiller, R., Stieger, J., Imer, D., Merbold, L.,
1001 & Buchmann, N. (2013). Corrigendum: Contrasting response of grassland versus forest
1002 carbon and water fluxes to spring drought in Switzerland. *Environmental Research Letters*,
1003 *8*, 035007
- 1004 Wolf, S., Keenan, T.F., Fisher, J.B., Baldocchi, D.D., Desai, A.R., Richardson, A.D., Scott, R.L.,
1005 Law, B.E., Litvak, M.E., Brunzell, N.A., Peters, W., & van der Laan-Luijkx, I.T. (2016).

- 1006 Warm spring reduced carbon cycle impact of the 2012 US summer drought. *Proceedings of*
1007 *the National Academy of Sciences of the United States of America*, 113, 5880-5885
- 1008 Xiao, X.M., Hollinger, D., Aber, J., Goltz, M., Davidson, E.A., Zhang, Q.Y., & Moore, B. (2004a).
1009 Satellite-based modeling of gross primary production in an evergreen needleleaf forest.
1010 *Remote Sensing of Environment*, 89, 519-534
- 1011 Xiao, X.M., Zhang, Q.Y., Braswell, B., Urbanski, S., Boles, S., Wofsy, S., Berrien, M., & Ojima, D.
1012 (2004b). Modeling gross primary production of temperate deciduous broadleaf forest using
1013 satellite images and climate data. *Remote Sensing of Environment*, 91, 256-270
- 1014 Xin, Q., Broich, M., Suyker, A.E., Yu, L., & Gong, P. (2015). Multi-scale evaluation of light use
1015 efficiency in MODIS gross primary productivity for croplands in the Midwestern United
1016 States. *Agricultural and Forest Meteorology*, 201, 111-119
- 1017 Yuan, W., Cai, W., Chen, Y., Liu, S., Dong, W., Zhang, H., Yu, G., Chen, Z., He, H., Guo, W., Liu,
1018 D., Liu, S., Xiang, W., Xie, Z., Zhao, Z., & Zhou, G. (2016). Severe summer heatwave and
1019 drought strongly reduced carbon uptake in Southern China. *Scientific Report*, 6, 18813
- 1020 Yuan, W., Cai, W., Xia, J., Chen, J., Liu, S., Dong, W., Merbold, L., Law, B., Arain, A., Beringer, J.,
1021 Bernhofer, C., Black, A., Blanken, P.D., Cescatti, A., Chen, Y., Francois, L., Gianelle, D.,
1022 Janssens, I.A., Jung, M., Kato, T., Kiely, G., Liu, D., Marcolla, B., Montagnani, L., Raschi,
1023 A., Rouspard, O., Varlagin, A., & Wohlfahrt, G. (2014). Global comparison of light use
1024 efficiency models for simulating terrestrial vegetation gross primary production based on
1025 the LaThuile database. *Agricultural and Forest Meteorology*, 192-193, 108-120
- 1026 Yuan, W.P., Cai, W.W., Nguy-Robertson, A.L., Fang, H.J., Suyker, A.E., Chen, Y., Dong, W.J., Liu,
1027 S.G., & Zhang, H.C. (2015). Uncertainty in simulating gross primary production of cropland
1028 ecosystem from satellite-based models. *Agricultural and Forest Meteorology*, 207, 48-57
- 1029 Zhang, Y., Song, C., Sun, G., Band, L.E., Noormets, A., & Zhang, Q. (2015). Understanding
1030 moisture stress on light use efficiency across terrestrial ecosystems based on global flux and
1031 remote-sensing data. *Journal of Geophysical Research: Biogeosciences*, 120, 2053-2066
- 1032 Zhang, Y., Xiao, X., Jin, C., Dong, J., Zhou, S., Wagle, P., Joiner, J., Guanter, L., Zhang, Y., Zhang,
1033 G., Qin, Y., Wang, J., & Moore, B. (2016a). Consistency between sun-induced chlorophyll
1034 fluorescence and gross primary production of vegetation in North America. *Remote Sensing*
1035 *of Environment*, 183, 154-169
- 1036 Zhang, Y., Xiao, X., Wu, X., Zhou, S., Zhang, G., Qin, Y., & Dong, J. (2017). A global moderate
1037 resolution dataset of gross primary production of vegetation for 2000–2016. *Scientific Data*,
1038 4, 170165
- 1039 Zhang, Y., Xiao, X.M., Zhou, S., Ciais, P., McCarthy, H., & Luo, Y.Q. (2016b). Canopy and
1040 physiological controls of GPP during drought and heat wave. *Geophysical Research Letters*,
1041 43, 3325-3333
- 1042 Zhu, Q., Zhuang, Q., Henze, D., Bowman, K., Chen, M., Liu, Y., He, Y., Matsueda, H., Machida, T.,
1043 Sawa, Y., & Oechel, W. (2014). Constraining terrestrial ecosystem CO₂ fluxes by
1044 integrating models of biogeochemistry and atmospheric transport and data of surface carbon
1045 fluxes and atmospheric CO₂ concentrations. *Atmospheric Chemistry and Physics*
1046 *Discussions*, 14, 22587-22638
- 1047 Zscheischler, J., Mahecha, M.D., von Buttlar, J., Harmeling, S., Jung, M., Rammig, A., Randerson,
1048 J.T., Scholkopf, B., Seneviratne, S.I., Tomelleri, E., Zaehle, S., & Reichstein, M. (2014). A
1049 few extreme events dominate global interannual variability in gross primary production.
1050 *Environmental Research Letters*, 9, doi:10.1088/1748-9326/1089/1083/035001
- 1051
- 1052



1053

1054 **Fig. 1.** (a) Land cover map of CONUS derived from MCD12Q1 in 2011 and (b) the C₄ crop
 1055 percentage within a 500-m MODIS pixel derived from 30-m cropland data layer.

1056 Abbreviations denote the IGBP land-use classes. WAT: Water, ENF: Evergreen Needleleaf

1057 Forest, EBF: Evergreen Broadleaf Forest, DNF: Deciduous Needleleaf Forest, DBF:

1058 Deciduous Broadleaf Forest, MF: Mixed Forest, CS: Closed Shrublands, OS: Open

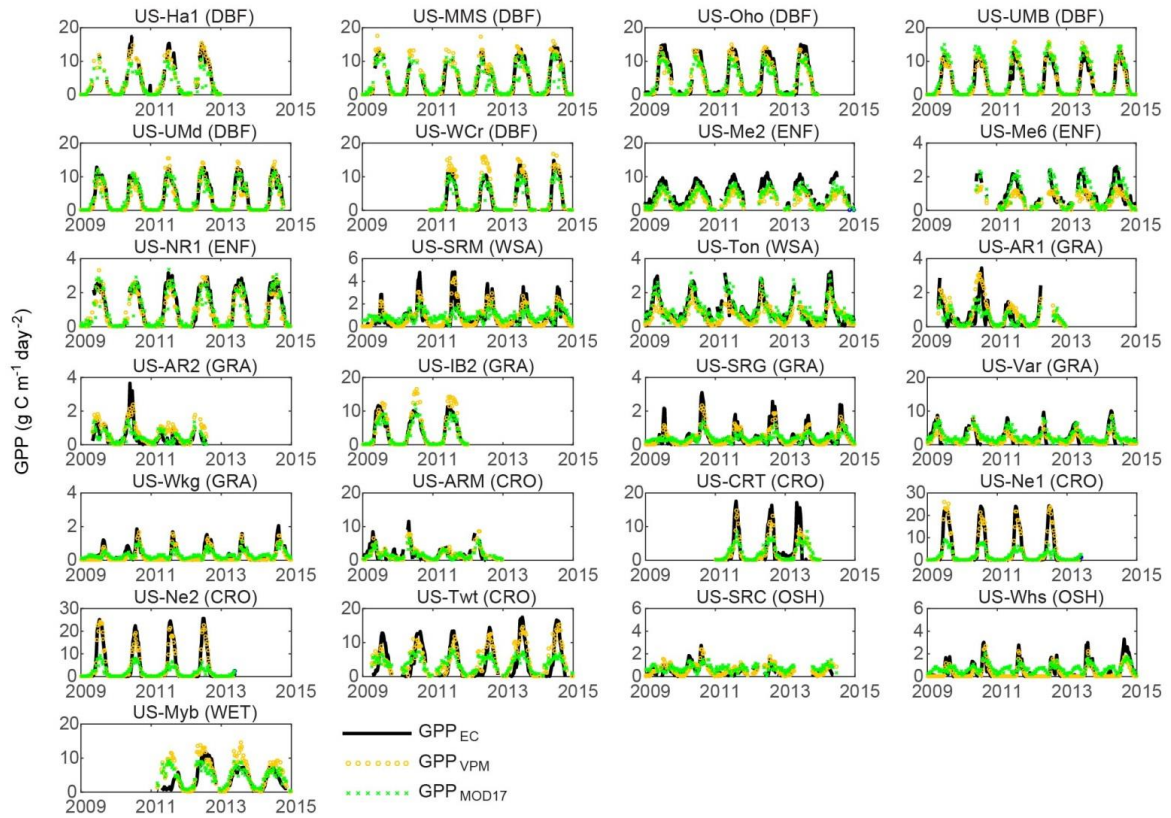
1059 Shrublands, WS: Woody Shrublands, SAV: Savannas, GRA: Grasslands, PW: permanent

1060 wetlands, CRO: Croplands, UB: Urban and Built-up, MOS: Cropland/Natural vegetation

1061 mosaic; SNO: Snow and Ice; BAR: Barren or sparsely vegetated. In Fig. 1a, we also labeled

1062 the locations of the eddy covariance flux tower sites used in this study.

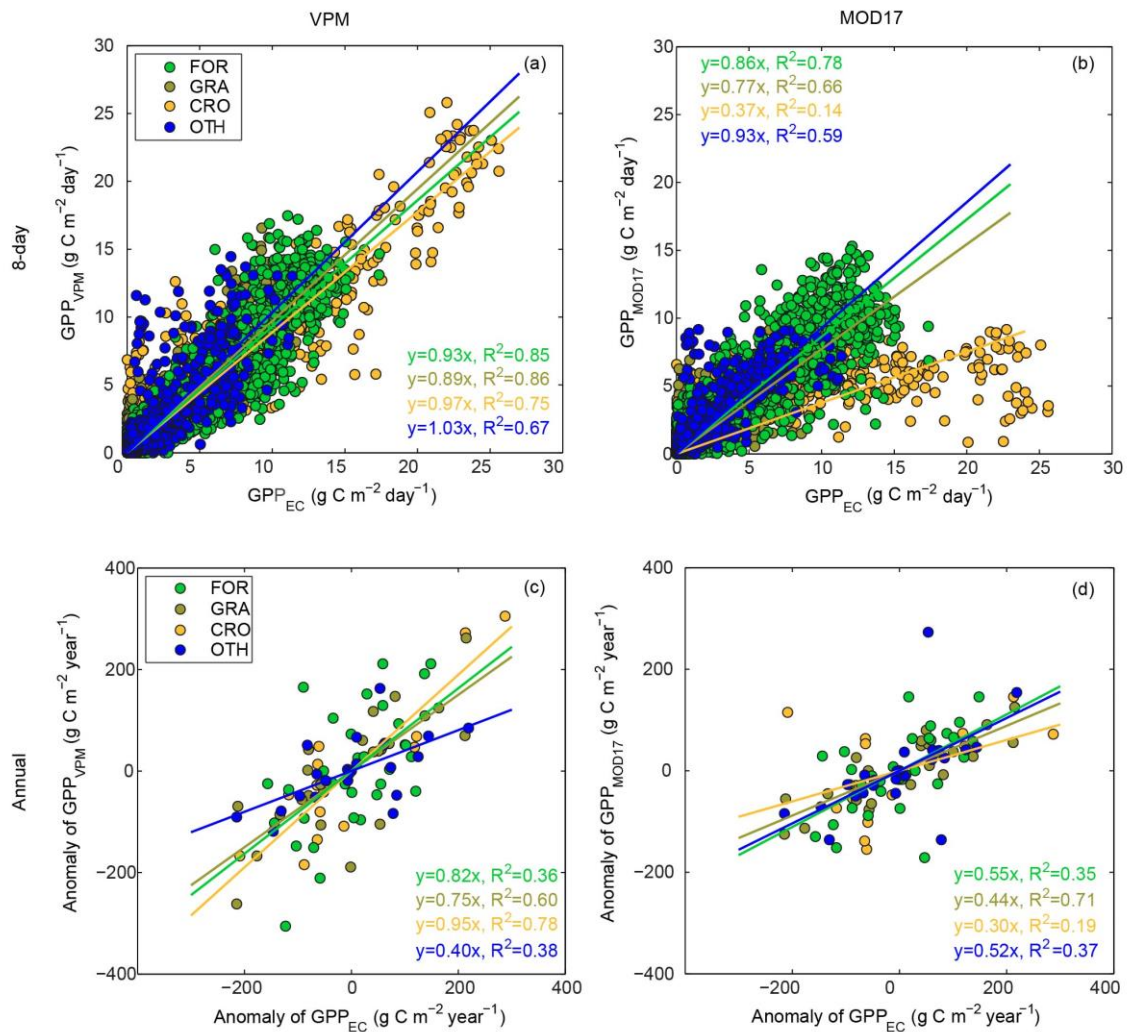
1063



1064

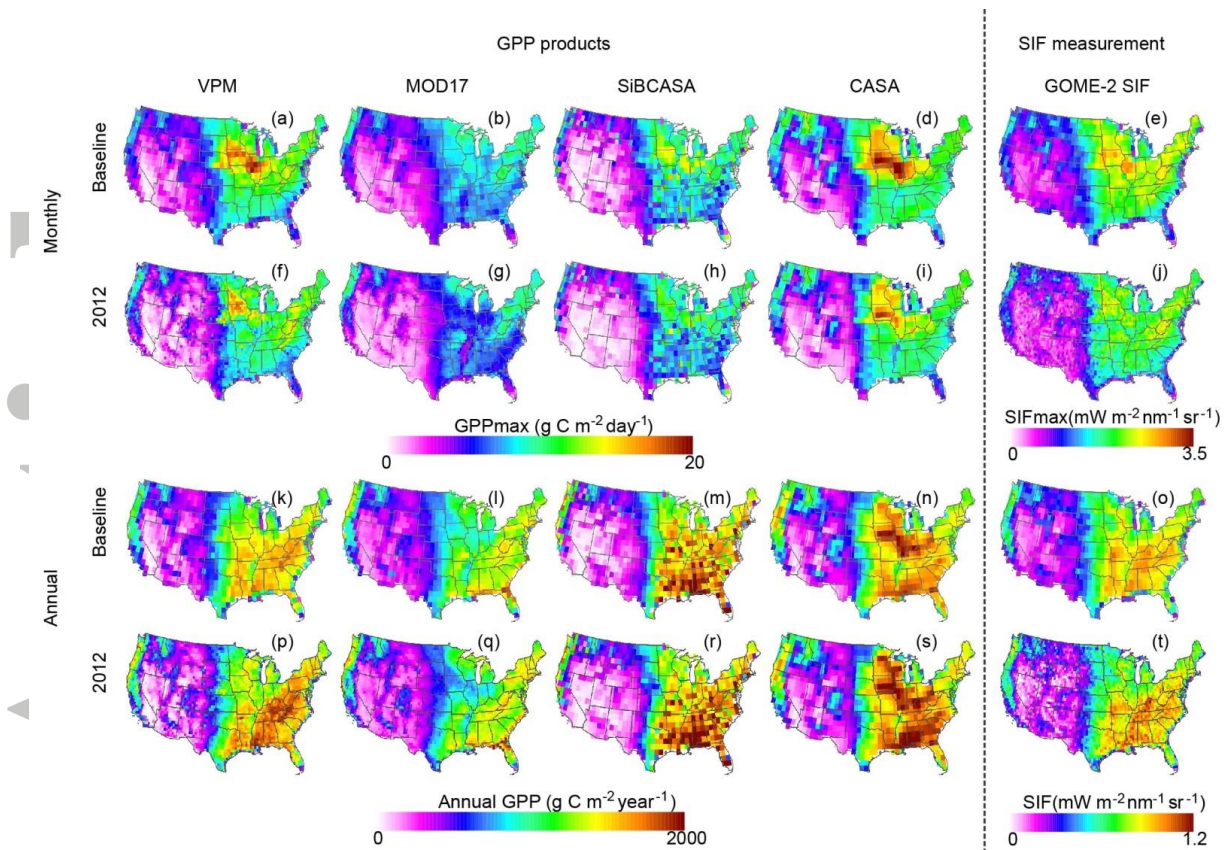
1065 **Fig. 2.** Seasonal dynamics and interannual variations of the tower-based GPP (GPP_{EC}), GPP
 1066 simulated by VPM (GPP_{VPM}), and GPP simulated by MOD17 (GPP_{MOD17}) at 25 flux sites at
 1067 8-day intervals (please note the different y-axis scales).

1068



1069

1070 **Fig. 3.** Comparison of GPP_{EC} , GPP_{VPM} , and GPP_{MOD17} across eddy covariance flux tower
 1071 sites (forest, grassland, cropland, and others) during 2008 to 2014: (a) 8-day GPP_{EC} and
 1072 GPP_{VPM} , (b) 8-day GPP_{EC} and GPP_{MOD17} , (c) anomaly of annual GPP_{EC} and GPP_{VPM} , and (d)
 1073 anomaly of annual GPP_{EC} and GPP_{MOD17} . FOR: forests, CRO: croplands, GRA: grasslands,
 1074 OTH: other types. When all the sites were combined, the relationship between GPP_{VPM} and
 1075 GPP_{EC} was $y = 0.92 x$ ($R^2 = 0.84$, $RMSE = 1.7 \text{ g C m}^{-2} \text{ d}^{-1}$) at the 8-day time scale, while the
 1076 relationship between GPP_{MOD17} and GPP_{EC} was $y = 0.68 x$ ($R^2 = 0.55$, $RMSE = 2.6 \text{ g C m}^{-2}$
 1077 day^{-1}) at the 8-day time scale. At the inter-annual scale, the relationship between the annual
 1078 anomaly of GPP_{VPM} and GPP_{EC} is $y = 0.73 x$ ($R^2 = 0.48$) while the relationship between the
 1079 annual anomaly of GPP_{MOD17} and GPP_{EC} was $y = 0.45 x$ ($R^2 = 0.37$).

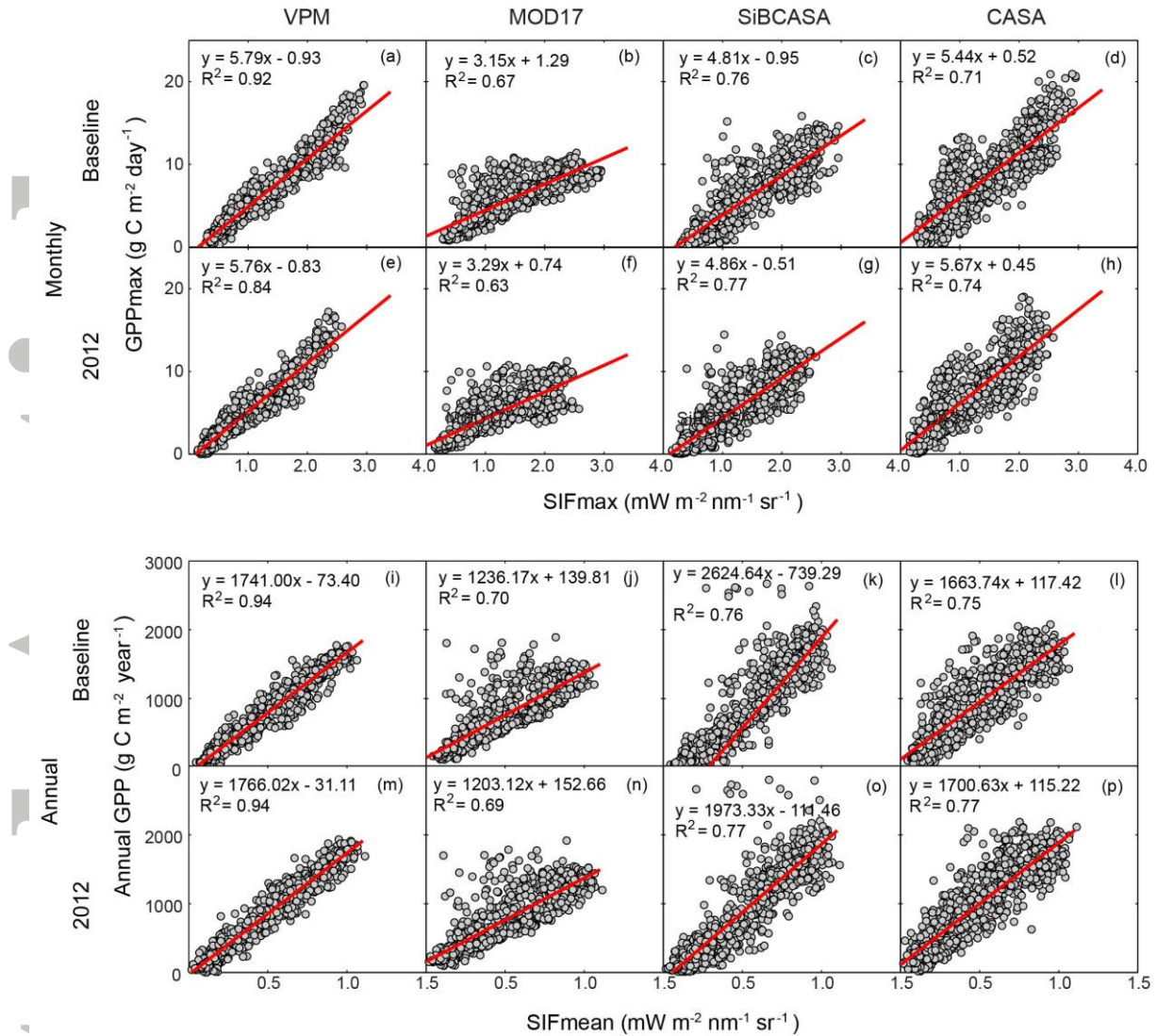


1080

1081 **Fig. 4.** Spatial distribution of maximum monthly mean GPP (a–d; f–i) from GPP models
 1082 (VPM, MOD17, SiB-CASA and CASA) and maximum monthly mean SIF (e, j) from
 1083 GOME-2 (e, j) in the baseline years (the average of 2008, 2009, 2010, 2013, 2014) and
 1084 drought year 2012, and spatial distributions of annual GPP (k–n; p–s) from GPP models and
 1085 annual mean SIF from GOME-2 (o, t) in the baseline years and drought year 2012.

1086

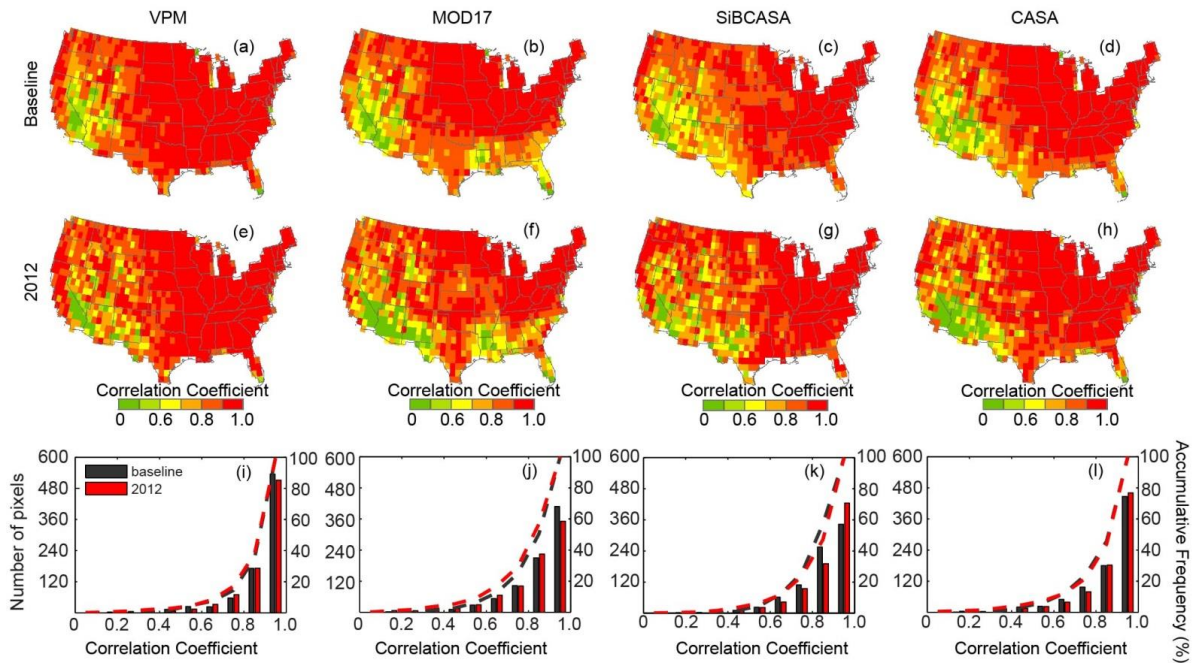
Accepted



1087

1088 **Fig. 5.** Relationships between the maximum monthly mean GPP (a–d; e–h) from GPP models
 1089 (VPM, MOD17, SiBCASA and CASA) and monthly mean SIF from GOME-2 for each pixel
 1090 across CONUS during the baseline years (the average of 2008, 2009, 2010, 2013 and 2014)
 1091 and drought year 2012, and relationship between total annual GPP (i–l; m–p) from GPP
 1092 models (VPM, MOD17, SiBCASA, and CASA) and mean annual SIF from GOME-2 in the
 1093 baseline year (the average of 2008, 2009, 2010, 2013 and 2014) and drought year 2012 (all
 1094 of the relationships are significant with $p < 0.001$).

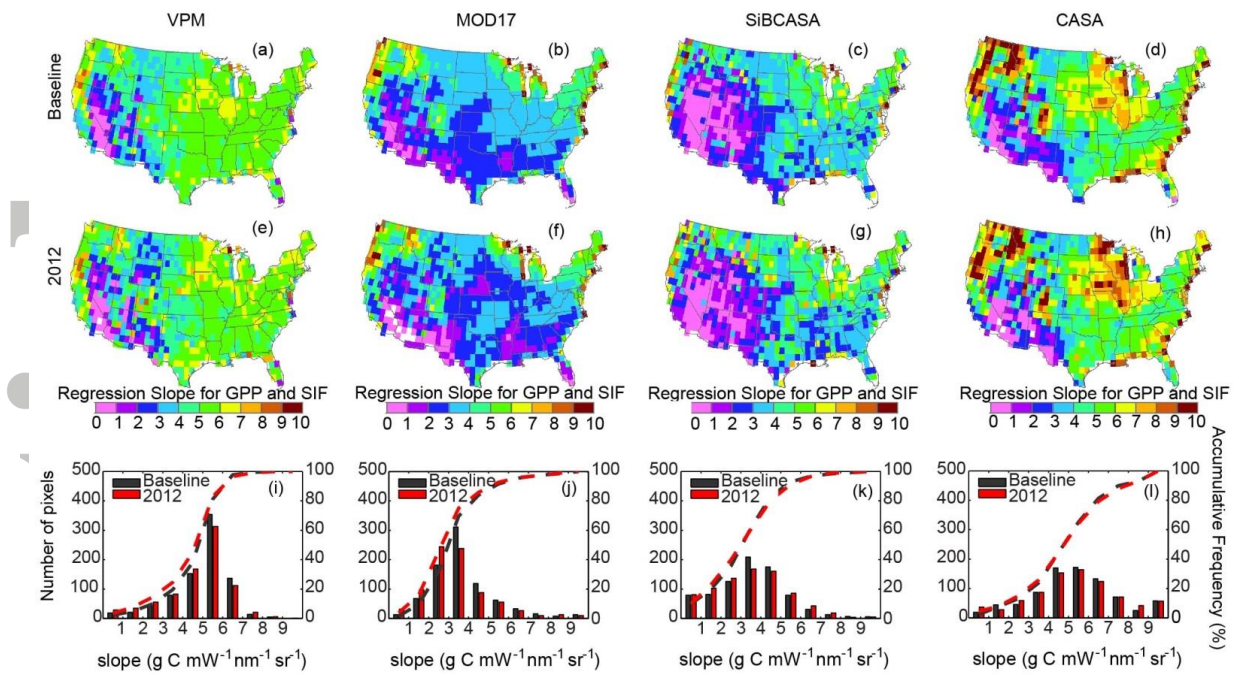
1095



1096

1097 **Fig. 6.** Spatial distribution of Pearson correlation coefficient between monthly SIF and GPP
 1098 products from VPM, MOD17, SiBCASA, and CASA for baseline year (the average of 2008,
 1099 2009, 2010, 2013, and 2014) and drought year 2012, and the corresponding frequency
 1100 distribution (black and red bars) and accumulative frequency (black and red dashed lines) of
 1101 the Pearson correlation coefficient for the four models in the baseline years and 2012.

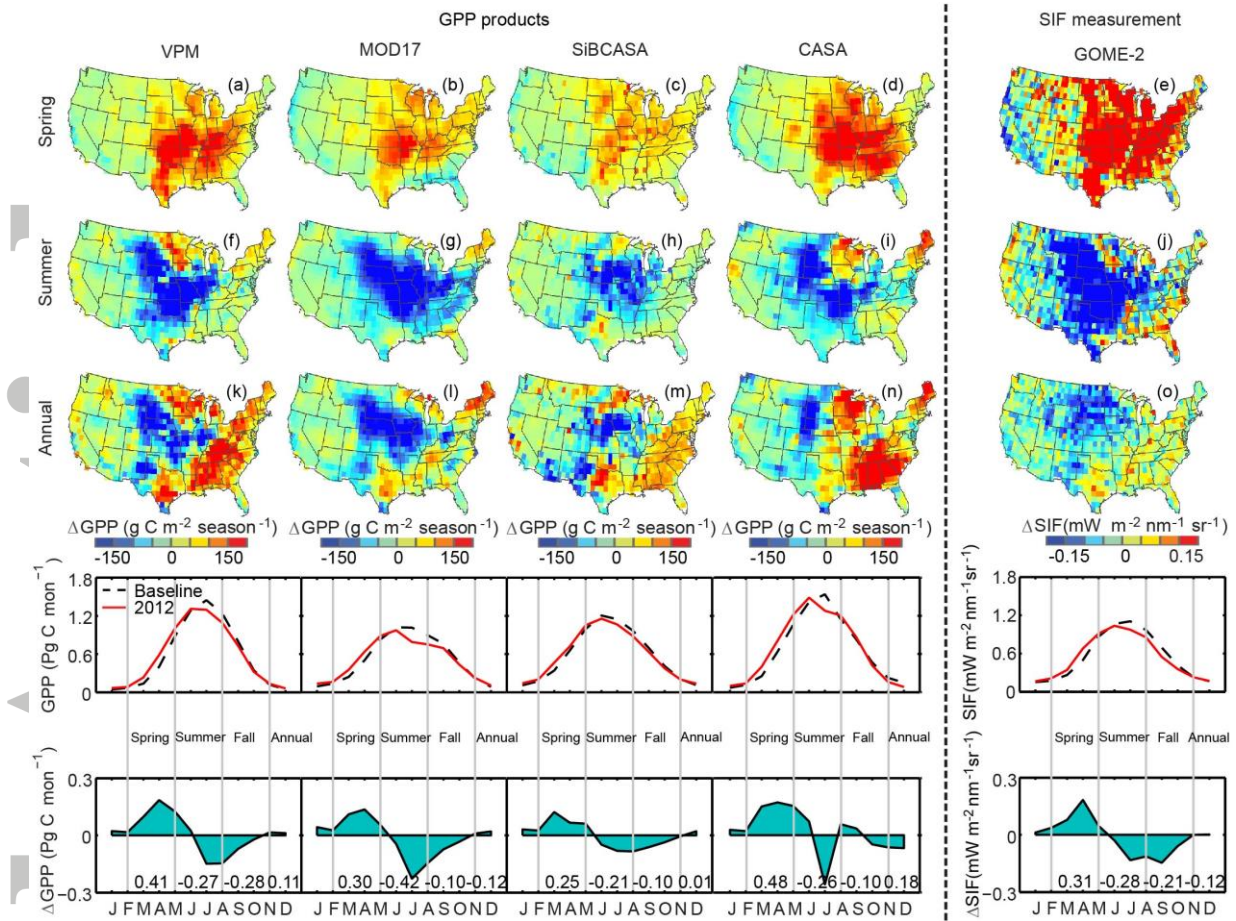
1102



1103

1104 **Fig. 7.** Spatial distribution of the regression slope between monthly SIF and GPP products
 1105 from VPM, MOD17, SiBCASA, and CASA for the baseline year (the average of 2008, 2009,
 1106 2010, 2013, and 2014) and drought year 2012, and the corresponding frequency distribution
 1107 (black and red bars) and accumulative frequency (black and red dashed lines) of the Pearson
 1108 correlation coefficient for the four models in the baseline years and 2012.

1109



1110

1111

Fig. 8. Spatial-temporal anomalies of GPP_{VPM} , GPP_{MOD17} , $GPP_{SiBCASA}$, GPP_{CASA} , and SIF

1112

during spring, summer, and annually across CONUS in 2012 relative to the baseline (2008,

1113

2009, 2010, 2013 and 2014). Seasonal cycle and anomaly of total monthly GPP_{VPM} ,

1114

GPP_{MOD17} , $GPP_{SiBCASA}$, GPP_{CASA} and SIF in 2012 relative to the baseline. Numbers shown in

1115

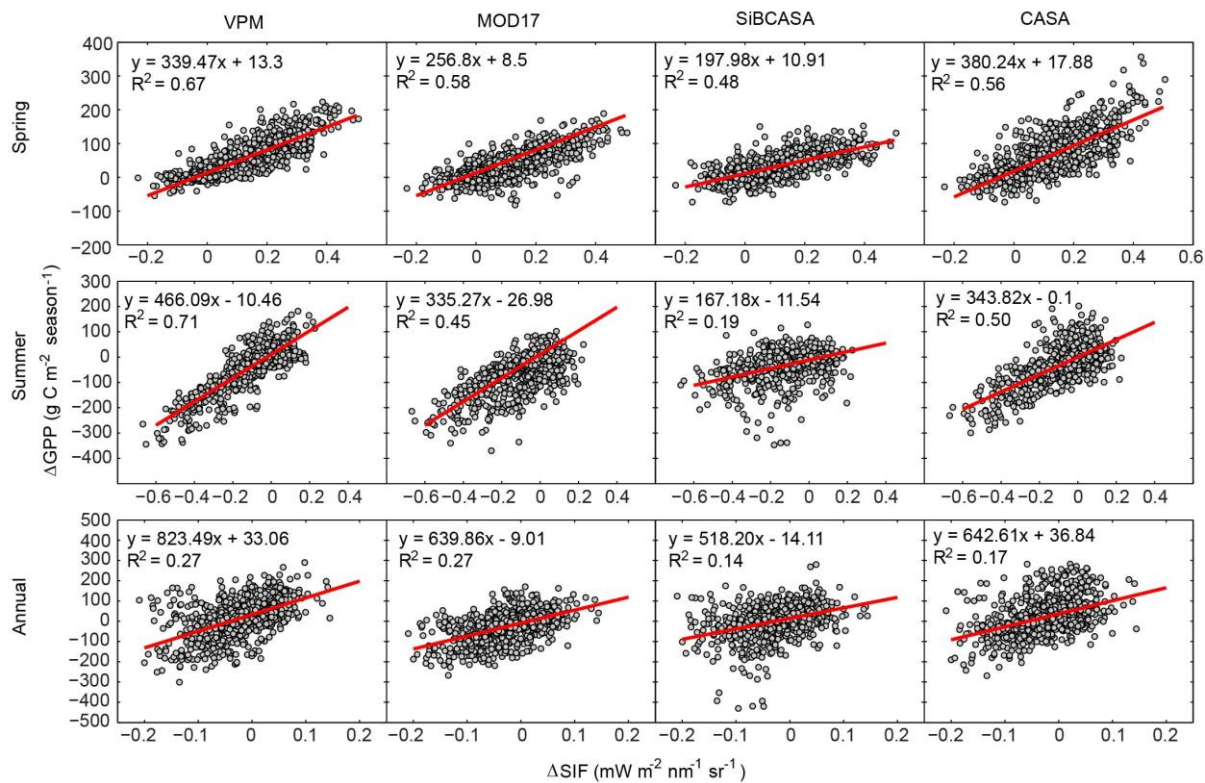
the last row of graphs are the anomaly of total GPP in spring (March–May), summer (June–

1116

August), fall (September–November) and the whole year (January to December).

1117

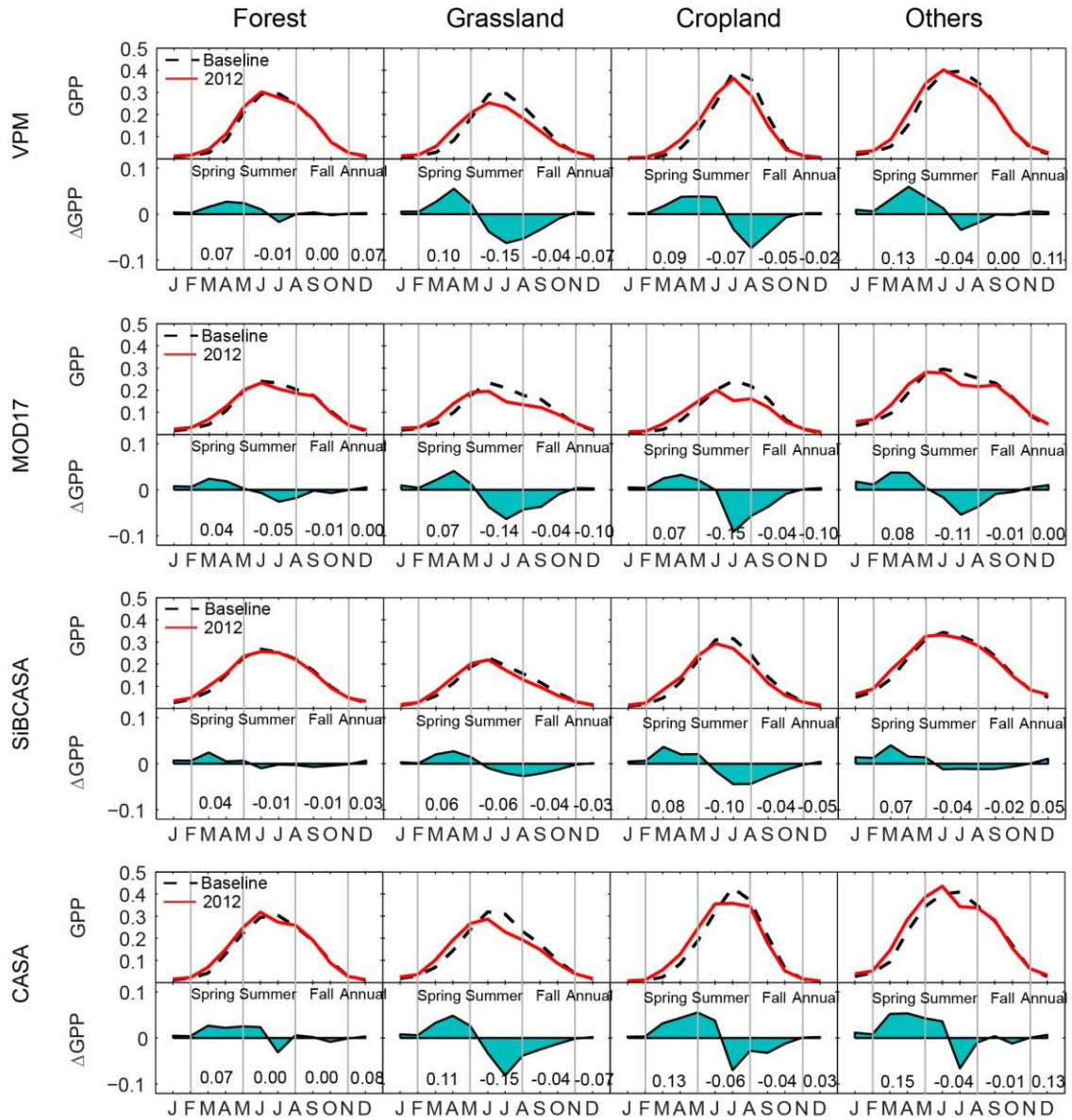
Accepted Article



1118

1119 **Fig. 9.** Correlation between the anomaly of seasonal/annual GPP from GPP models (VPM,
 1120 MOD17, SiBCASA, and CASA) and the anomaly of seasonal/annual mean SIF from GOME-
 1121 2 across CONUS during the baseline years (the average of 2008, 2009, 2010, 2013 and 2014)
 1122 and drought year 2012 (all of the correlations are significant with $p < 0.001$).

1123

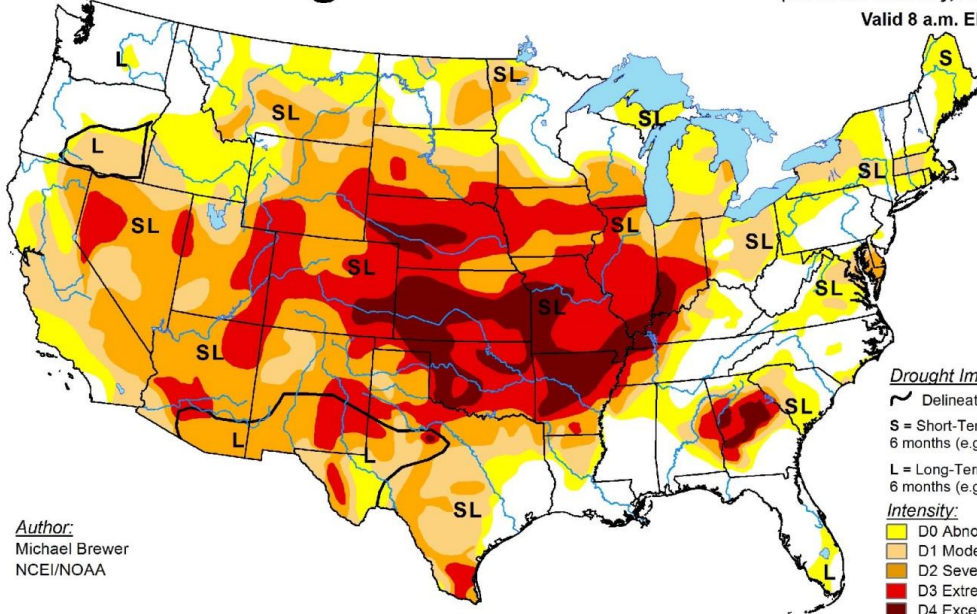


1124
 1125 **Fig. 10.** Seasonal cycle and anomaly of total monthly GPP_{VPM} , $GPP_{SiBCASA}$, GPP_{CASA} , and
 1126 GPP_{MOD17} in (a) forest, (b) grassland, (c) cropland and (d) others. Numbers shown in the
 1127 bottom panel in each row are the anomalies of total GPP for each biome in spring (March–
 1128 May), summer (June–August), fall (September–November) and the whole year.

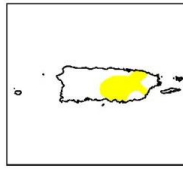
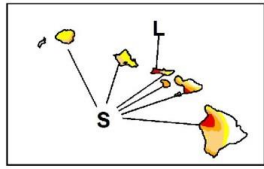
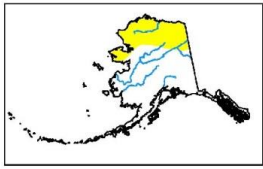
1129

U.S. Drought Monitor

August 14, 2012
(Released Thursday, Aug. 16, 2012)
Valid 8 a.m. EDT



Author:
Michael Brewer
NCEI/NOAA



USDA
National Drought Mitigation Center
NOAA
<http://droughtmonitor.unl.edu/>

1130

1131 **Fig. 11.** Drought-affected areas over CONUS on August 14, 2012 .

1132

Accepted

1133 **Table 1.** Name, location, vegetation type, and available years (within 2008–2014 study period) of 25 eddy covariance flux tower sites in this
 1134 study. RMSE, R^2 , and slope are the root mean square error, coefficient of determination, and regression slope of the regression analysis,
 1135 respectively, between tower-derived GPP and simulated GPP from VPM and MOD17.

Site ID	Latitude	Longitude	IGBP	Time	slope		R^2		RMSE (g C m ⁻² d ⁻¹)		References	DOI
					VPM	MOD17	VPM	MOD17	VPM	MOD17		
US-Ha1	42.5378	-72.1715	DBF	2009–2012	0.93	0.66	0.93	0.74	1.32	2.89	(Urbanski et al. 2007)	http://dx.doi.org/10.17190/AMF/1246059
US-MMS	39.3232	-86.4131	DBF	2009–2014	1.07	0.85	0.91	0.71	1.58	2.33	(Schmid et al. 2000)	http://dx.doi.org/10.17190/AMF/1246080
US-Oho	41.5545	-83.8438	DBF	2009–2013	0.87	0.77	0.92	0.83	1.63	2.37	(van Gorsel et al. 2009)	http://dx.doi.org/10.17190/AMF/1246089
US-UMB	45.5598	-84.7138	DBF	2009–2014	1.09	1.20	0.96	0.93	1.15	1.87	(Gough et al. 2008)	http://dx.doi.org/10.17190/AMF/1246107
US-Umd	45.5625	-84.6975	DBF	2009–2014	0.91	0.90	0.88	0.84	1.64	1.70	(Gough et al. 2013)	http://dx.doi.org/10.17190/AMF/1246134
US-WCr	45.8059	-90.0799	DBF	2011–2014	1.25	0.84	0.90	0.80	2.46	2.03	(Cook et al. 2004)	http://dx.doi.org/10.17190/AMF/1246111
US-Me2	44.4523	-121.5574	ENF	2009–2014	0.58	0.72	0.74	0.79	2.81	2.08	(Law et al. 2004)	http://dx.doi.org/10.17190/AMF/1246076
US-Me6	44.3233	-121.6078	ENF	2010–2014	0.56	0.95	0.51	0.56	1.53	1.26	(Law et al. 2000)	http://dx.doi.org/10.17190/AMF/1246128
US-NR1	40.0329	-105.5464	ENF	2009–2014	0.84	0.91	0.86	0.84	1.04	1.03	(Monson et al. 2002)	http://dx.doi.org/10.17190/AMF/1246088
US-SRM	31.8214	-110.8661	WSA	2009–2014	0.90	0.61	0.74	-1.18	0.49	0.81	(Scott et al. 2009)	http://dx.doi.org/10.17190/AMF/1246104
US-Ton	38.4316	-120.9660	WSA	2009–2014	0.68	1.01	0.61	0.73	1.28	0.91	(Baldocchi et al. 2004)	http://dx.doi.org/10.17190/AMF/1245971
US-AR1	36.4267	-99.4200	GRA	2009–2012	1.07	0.59	0.55	0.06	1.35	1.35	-	http://dx.doi.org/10.17190/AMF/1246137
US-AR2	36.6358	-99.5975	GRA	2009–2012	1.08	0.62	0.43	-0.12	1.14	1.20	-	http://dx.doi.org/10.17190/AMF/1246138
US-IB2	41.8406	-88.2410	GRA	2009–2011	1.21	0.84	0.87	0.86	2.14	1.52	(Matamala et al. 2008)	http://dx.doi.org/10.17190/AMF/1246066
US-SRG	31.7894	-110.8277	GRA	2009–2014	0.78	0.51	0.69	-0.35	0.75	1.16	(Scott et al. 2015)	http://dx.doi.org/10.17190/AMF/1246154
US-Var	38.4133	-120.9507	GRA	2009–2014	0.66	0.88	0.66	0.42	1.71	1.65	(Ma et al. 2007)	http://dx.doi.org/10.17190/AMF/1245984
US-Wkg	31.7365	-109.9419	GRA	2009–2014	0.76	0.63	0.82	0.39	0.54	0.69	(Scott et al. 2010)	http://dx.doi.org/10.17190/AMF/1246112
US-ARM	36.6058	-97.4888	CRO	2009–2012	0.79	0.64	0.57	0.47	1.46	1.56	(Fischer et al. 2007)	http://dx.doi.org/10.17190/AMF/1246027
US-CRT	41.6285	-83.3471	CRO	2011–2013	0.68	0.45	0.78	0.64	3.00	4.23	(Chu et al. 2014)	http://dx.doi.org/10.17190/AMF/1246156

US-Ne1	41.1651	-96.4766	CRO	2009–2012	0.96	0.31	0.95	0.51	1.80	7.62	(Suyker et al. 2005)	http://dx.doi.org/10.17190/AMF/1246084
US-Ne2	41.1649	-96.4701	CRO	2009–2012	0.89	0.29	0.96	0.41	1.90	8.19	(Suyker et al. 2005)	http://dx.doi.org/10.17190/AMF/1246085
US-Twt	38.1087	-121.6530	CRO	2009–2014	0.87	0.53	0.43	-0.93	3.17	4.24	(Hatala et al. 2012)	http://dx.doi.org/10.17190/AMF/1246140
US-SRC	31.9083	-110.8395	OSH	2009–2014	0.97	0.99	0.32	-1.31	0.39	0.42	(Cavanaugh et al. 2011)	http://dx.doi.org/10.17190/AMF/1246127
US-Whs	31.7438	-110.0522	OSH	2009–2014	0.70	0.71	0.72	-0.28	0.45	0.56	(Scott et al. 2015)	http://dx.doi.org/10.17190/AMF/1246113
US-Myb	38.0498	-121.7651	WET	2011–2014	1.27	0.92	0.36	-0.31	3.49	2.85	(Sturtevant et al. 2016)	http://dx.doi.org/10.17190/AMF/1246139

1136

1137

1138 **Table 2.** The anomaly of total GPP between 2012 and the baseline (the average of 2008,
 1139 2009, 2010, 2013 and 2014) in spring (March–May), summer (June–August), fall
 1140 (September–November) and the whole year. The uncertainty range of the anomaly was
 1141 calculated as the standard deviation (SD) of the anomaly between 2012 and different
 1142 baselines. We randomly chose at least three years from the year 2008, 2009, 2010, 2013 and
 1143 2014 to calculate the baseline, so there are 16 options ($C_5^3 + C_5^4 + C_5^5$).

Anomaly of GPP (Pg C)	VPM	MODIS	CASA	SiBCASA	Anomaly of SIF ($\text{mW m}^{-2} \text{nm}^{-1} \text{sr}^{-1}$)
Spring	0.41 ± 0.04	0.30 ± 0.03	0.48 ± 0.05	0.25 ± 0.03	0.31 ± 0.05
Summer	-0.27 ± 0.05	-0.42 ± 0.02	-0.26 ± 0.06	-0.21 ± 0.04	-0.28 ± 0.05
Annual	0.11 ± 0.08	-0.12 ± 0.02	0.18 ± 0.10	0.01 ± 0.08	-0.12 ± 0.10

1144

1145

1146 **Table 3.** The anomaly of total GPP estimates from VPM, MOD17, SiBCASA and CASA for
 1147 different biomes between 2012 and the baseline (the average of 2008, 2009, 2010, 2013 and
 1148 2014) in spring (March–May), summer (June–August), fall (September–November) and the
 1149 whole year.

Anomaly of GPP (Pg C)		Spring	Summer	Fall	Annual
VPM	Forest	0.07	-0.01	0.00	0.07
	Grassland	0.10	-0.15	-0.04	-0.07
	Cropland	0.09	-0.07	-0.05	-0.02
	Others	0.13	-0.04	0.00	0.11
MOD17	Forest	0.04	-0.05	-0.01	0.00
	Grassland	0.07	-0.14	-0.04	-0.10
	Cropland	0.08	-0.15	-0.04	-0.10
	Others	0.08	-0.11	-0.01	0.00
SiBCASA	Forest	0.04	-0.01	-0.01	0.03
	Grassland	0.06	-0.06	-0.04	-0.03
	Cropland	0.08	-0.10	-0.04	-0.05
	Others	0.07	-0.04	-0.02	0.05
CASA	Forest	0.07	0.00	-0.01	0.08
	Grassland	0.11	-0.15	-0.04	-0.07
	Cropland	0.13	-0.06	-0.04	0.03
	Others	0.15	-0.04	-0.01	0.13

1150

1151 *Forest including: evergreen needleleaf forest, evergreen broadleaf forest, deciduous
 1152 broadleaf forest, deciduous needleleaf forest, mixed forest; Grassland: grassland; Cropland:
 1153 cropland; Others: closed shrublands, open shrublands, savannahs, woody savannahs,
 1154 permanent wetlands, cropland/natural vegetation mosaics.

1155